BACHELOR THESIS

"Light Emission of an Ion Getter Pump in Connection with the ALPS-II Experiment"

Severin Wipf
Ernst-Abbe-Fachhochschule Jena
Physikalische Technik
633912

September 5, 2013

BACHELOR THESIS

"Light Emission of an Ion Getter Pump in Connection with the ALPS-II Experiment"

Severin Wipf
Ernst-Abbe-Fachhochschule Jena
Physikalische Technik
633912
September 5, 2013
Created at: Deutsches Elektronen-Synchrotron Hamburg

Ernst-Abbe-Fachhochschule Jena
Hochschule für angewandte Wissenschaften

First supervisor: Prof. Dr. Harald Bergner, Ernst, Ernst-Abbe-Fachhochschule Jena

Second supervisor: PostDoc Babette Döbrich, Deutsches Elektronen-Synchrotron Hamburg

Severin Wipf
Physikalische Technik
Ernst-Abbe-Fachhochschule-Jena

STATUTORY DECLARATION

I declare that I have authored this thesis independently, that I have not used other than the declared sources / resources, and that I have explicitly marked all material which has been quoted either literally or by content from the used sources

.....	.....
date	signature

I want to thank very much...

Ingrid Wipf
Jan-Eike von Seggern
Babette Döbrich
Reza Hodajerdi
Dieter Trines
Axel Lindner
Axel Knabbe
and the remaining members of ALPS-II

...for helping me a lot writing down this thesis.

Contents

1 List of Tables

List of Tables

2 List of Figures

List of Figures

3 Index

3.1 Abbreviations

AC	Alternating Current
ADU	Analog to Digital Unit
ALPS	Any Light Particle Search
CCD	Charge Coupled Device
CERN	Conseil Européen pour la Recherche Nucléaire
cw	continuous wave
DC	Direct Current discharge
DESY	Deutsches Elektronen-Synchrotron
FWHM	Full Width Half Maximum
HERA	Hadron-Elektron-Ring-Anlage
LHC	Large Hadron Collider
M	Measurement
MOS	Metal Oxide Semiconductor structure
Nd:YAG	Neodymium-doped Yttrium Aluminum Garnet
PIXIS	PIXIS1024B
PX	Pixels
QE	Quantum Efficiency
RGA	Residual Gas Analyzer
SBIG	SBIG-ST402ME
SRS	Standford Research System
TES	Transition Edge Sensor
WISP	Weakly Interacting Sub ev Particle

3.2 Mathematical Symbols [Unit]

A_{ch}	area of the exposed chip $[m^2]$
A_{sp}	area element on hemisphere $[m^2]$
B	magnetic flux density $[T]$
c	speed of light $[\frac{m}{s}]$
d	specific distances $[m]$
d_{ch}	distance between CCD chip and camera adaptive $[m]$
e	elementary charge $[C]$
E_{bin}	atomic binding energy $[J]$
E_c, E_v, E_{vac}	energy levels conduction band, valence band, vacuum $[J]$
E_g	band gap energy $[J]$
E_i	ionization energy of an atom $[J]$
E_{kin}	kinetic energy $[J]$
E_{Ph}	photon energy $[J]$
E_R	Rydberg energy $[J]$
E_{rot}, E_{vib}	energies of rotation and vibration $[J]$
E, E_x, E_y	electric field intensity $[\frac{V}{m}]$
f	frequency $[\frac{1}{s}]$
f_L	focal length $[m]$
G	electrical gain [ ]
h	Planck constant $[J \cdot s]$
I	electrical current $[A]$
$I(r), I_r$	light intensity of wavelength range r $[\frac{W}{sr}]$
I_{AL}	light intensity $[\frac{W}{sr}]$
I_{dt}	light intensity (detected, representative) $[ADU]$
I_{img}	percentage of imaged light intensity [%]
I_{mi}	molecular moment of inertia $[N \cdot m]$
I_{pre}	light intensity (pressure depended) $[ADU]$
J	integer quantum number of rotation [ ]
k	integer quantum number of oscillation [ ]
k_B	Boltzmann constant $[\frac{J}{K}]$
k_{ew}	wave number electron wave $[\frac{1}{m}]$
L	resonator length $[m]$
m, m_A, m_e	mass, atom mass, electron mass $[kg]$
n	refractive index [ ]
n_m	number of measurement values [ ]
n_p, n_{cc}	density of particles, density of charge carriers $[m^{-3}]$
n_q	integer main quantum number [ ]
N_e	number of electrons [ ]

p	pressure $[bar]$
p_{ew}	momentum electron wave $[N \cdot s]$
q	charge of a particle $[C]$
QE, η	quantum efficiency [%]
r, r_l	distance between penning cells and chip, lens $[m]$
r_1, r_2	wavelength ranges [ ]
r_{p1}, r_{p2}	radii of the interacting particles $[m]$
R_1, R_2	curvature radii of the laser cavities $[m]$
N_{px}	number of exposed pixels [ ]
r_e	curvature radius of a moving electron $[m]$
r_A	atom radius $[m]$
R_{ch}	photon rate, detected by the chip $\left[\frac{photons}{s}\right]$
R_{gp}	photon rate, emitted by the ion getter pump $\left[\frac{photons}{s}\right]$
R_{pm}, R_{sm}	reflectivity of plane/spherical mirror [%]
s	standard deviation [used unit]
t, t_E	time, exposure time $[s]$
T	temperature $[°C]$
T_x	transmission coefficient of an attribute x [%]
U_{bd}	breakdown voltage $[V]$
U_i	internal atom energy $[J]$
δU	modification internal atom energy $[J]$
v_e	electron speed $\left[\frac{m}{s}\right]$
w_e	electron energy $[J]$
x_0	ionization path length $[m]$
x_{px}	mean per pixel averaged over all pixels $[ADU]$
Z	atomic number [ ]
α	first Townsend coefficient [ ]
γ	second Townsend coefficient [ ]
λ	wavelength of light $[m]$
$\lambda_p, \lambda_e, \lambda_{Ph}$	mean free path length of a gas particle, electron, photon $[m]$
ω	angular frequency $\left[\frac{1}{s}\right]$
Ω	electric field potential $[V]$
$\sigma_p, \sigma_e, \sigma_{Ph}$	cross-section of gas particle, electron, Photon $\left[m^2\right]$
σ	confidence interval [±used unit]
S	pumping speed $\left[\frac{l}{s}\right]$
$Ø$	diameter $[m]$

4 Introduction and Motivation

With todays modern physics and its latest results in research it is possible to determine the composition of the universe really accurately. Despite enormous technical progress regarding the achievement of more and more detailed measurement results and all the latest physical knowledge of the past years, we can assume with good certainty that dark matter exists, but it has been completely unclear what this dark matter consists of. Currently several experiments are carried out worldwide to prove postulated modules of the dark matter. A group of theoretically predicted particles which could constitute the dark matter are the so called "WISP'S"[1]. The experiment ALPS-II[2] searches with a "light-shining-through-a-wall" experimental set-up at the "Deutsches Elektronen-Synchrotron" in Hamburg, Germany, for the existence of such particles. This experiment has to be carried out in an ultra high vacuum. For the generation of such a vacuum one possibility is to employ ion getter vacuum pumps. Based on the functional principle of the experiment which will be explained more detailed in the course of this thesis only a very little share of light with a wavelength of λ=1064nm may occur in a vacuum pumped detection room. Due to this requirement it needs to be checked whether the existing ion getter pumps in general produce a relevant share of light. If this is the case, it must be ascertained whether this light includes wavelengths in the infrared range and especially light with a wavelength of λ=1064nm. For the accomplishment of this task an analysis of the residual gas spectrum in a vacuum chamber should be done to verify the composition of the gas pumped out by the ion getter pump. In the main part of this thesis aims at measurements of light intensity with two different CCD cameras. To test whether the ion getter pump really produces light, measurements of the total emitted light intensity will be carried out. If the results of these measurements prove the existence of light, further measurements with different wavelength filters will be taken: the intensities of infrared light and light with a wavelength of λ=1064nm shall be determined in terms of quantity. For the emitted light intensity in the range of all detectable wavelengths and wavelengths in the infrared range approximate experimental results are sufficient. The emitted intensity of light with a wavelength of light with λ=1064nm, however, should be determined as precisely as possible.

To increase the reliability of the achieved results, furthermore there will be two more series of measurements carried out. First the behavior of the light production under increasing pressure in the pump room will be examined. Finally, with the assistance of different wavelength filters it will approximately be determined, what the percentage distribution of the existing wavelength ranges of the emitted light is.

Chapter 5 integrates the experimental tests of this thesis into the ALPS-II experiment. Chapter 6 contains theoretical foundations of the functional principles of ion getter pumps, light emission of gases and the functional principle of a mass spectrum analyzer. Optical properties of semiconductors and based on them the functional principle of "CCD" sensors are explained in chapter 7. In chapter 8 first the experimental methods are described, followed by the demonstration and discussion of the results and evaluations of all the experiments carried out.

[1] Weakly Interacting Sub ev Particles
[2] Any Light Particle Search

5 The ALPS-II Experiment at DESY

Physical science can only characterize approximately 5 % of the constituents of the universe with the current standard-model of elementary particles. The remaining components are unexplored and postulated as dark matter (≈27%) and dark energy(≈ 68%)[3]. To achieve better knowledge about the cosmic ingredients is one of the strongest motivations of modern experimental and theoretical particle physics. This is proven by the huge public interest for the experiments at the LHC[4] at CERN, Switzerland, and the various means for experiments in high-energy-physics. For example many successful experiments with accelerated high-energy-particles contributed to develop the standard model of elementary particles at CERN. Despite the progression of this kind of physics and the new scientific knowledge about the established matter some observations of stars do contradict the theoretical predictions. One fact is that stars at the outskirts move too fast around the center of their galaxy. Because of the fast circular motion of these stars the radial force is higher than the theoretical calculated attraction force between the stars and their galaxy and the system would become unstable[2]. Thus it follows that there must be a non-visible mass which affects the movement of the observed stars called dark matter. Dark matter would only weakly interact with photons[5], and therefore it is not visible with scientific experimental equipment. But observations with "gravity lenses" indirectly suggest its existence: Light is deflected by gravitation of large masses. As a consequence of this effect it is possible to see objects in the universe which actually should be covered by nearer objects in the same line of sight. Some galaxies deflect this light more than it would be possible with their visible mass. This incident suggests the existence of dark matter as well[3]. The dark energy would explain why on the other hand the expansion of the universe gets accelerated.

At "Deutsches Elektronen-Synchrotron" (DESY) in Hamburg, Germany, a great number of scientists do research at the basic of particle-physics also. The Experiment "ALPS-II" at DESY tries to prove the existence of "WISPs" (weakly interacting sub-eV particles), especially of "Axion-like-particles". These hypothetical particles might explain the dark matter. They would have a very small mass and interact extremely weakly with matter. Because of these properties WISPs may have never been noticed in other particle-experiments. ALPS-II is the subsequent experiment of ALPS-I and differs from this mainly in better sensitivity of measurements. ALPS-I has reached the highest sensitivity in laboratory experimental photon-WISPs coupling in the world[4]. The basic idea of ALPS-II to prove that WISPs exist is a "light-shining-through a wall"-experiment. This setup should take advantage of photon-WISP interaction: A laser beam hits a lightproof wall. Before and behind the wall a strong magnetic field affects with up to B=2 T. Due to quantum physical coupling[6] a photon could transform into an Axion-like-particle. This WISP would not interact with the wall and pass through. In the second magnetic field the particle could transform back into a photon by the reverse process. Changes of the magnetic field strength would have a direct influence on the light quantity which passes through. These photons would have exactly the same physi-

[3] calculated with new results of Planck Satellite in 2013[1]
[4] Large Hadron Collider with a circumference of 26,7km
[5] emission and absorption
[6] by the influence of a virtual photon an Axion-like-particle should arise

cal properties[7]as the incident laser beam photons. Behind the wall it should be detected by a special "Transition-Edge-Sensor" with a sensitivity of at least $10^{-4}\frac{Photons}{second}$.

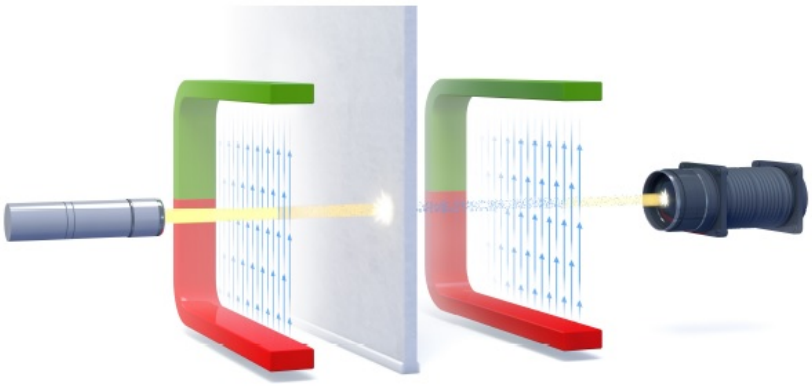

Figure 1: Sketch of laser beam hits a lightproof wall, magnetic field and detection-system of ALPS-II [4]

Figure 1 shows the basic structure of the ALPS-II experiment in principle. There are three stages of the experiment: "ALPS-IIa", which conduce to get a good control for the handling of the optical instruments and will be carried out in a laboratory. In a second test "ALPS-IIb" the experimental set-up will be reproduced magnified in the HERA-tunnel[8]. Finally in "ALPS-IIc" a magnetic field will be created with super conducting dipole magnets. Figure 19 shows the experimental set ups of ALPS-IIa, b and c.

For the photon beam a Nd:YAG[9] laser with a wavelength of 1064nm will be used. The narrow-band and frequency-stabilized Nd:YAG laser can operate in cw driving and provides a laser power of up to 35W. One optical resonator will be placed before and one behind the wall. The resonator in front of the wall (Production-cavity) gives the photons more opportunities to convert into a WISP. The second resonator (Regeneration-cavity) enhances the probability for reconversion of WISP in a detectable photon. Both resonators have equal lengths and have a hemispherical shape, and each of the plane mirrors are on the closer position to the wall.

They have to meet the stability criterion[5] for optical resonators:

$$0 \leq (1 - \frac{L}{R_1}) \cdot (1 - \frac{L}{R_2}) \leq 1 \tag{5.0.1}$$

with:

[7]wavelength, spin, interaction of a virtual photon from the magnetic field with a laser photon, polarization
[8]"Hadon-Electron-Ring-Anlage" of DESY with a circumference of 6,3km (construction for particle acceleration)
[9]Neodymium-doped Yttrium Aluminum Garnet; $Nd : Y_3Al_5O_12$

L – resonator length
R_1 – radius of curvature first mirror
R_2 – radius of curvature second mirror

With $R_2 = \infty$ for the plane mirrors the three ALPS-II experiments have the following cavity set-up parameters:

Experiment	resonator lengths L in m	R_1 in m
ALPS-IIa	10	$\geq 10m$
ALPS-IIb	100	$\geq 100m$
ALPS-IIc	100	$\geq 100m$

Table 1: Parameter for optical resonators in ALPS-II experiments

The regeneration-cavity has a power-build-up[10] of 40000. So one possibility would be that the plane mirror has a reflectivity of R_{pm}=100% and the spherical mirror R_{sm}=99.9975%. The production-cavity has a power buildup of 5000, that means for example R_{pm}=100% and R_{sm}=99.98%. But this calculations are only idealized theoretical thoughts. In reality the transmission T_m=100-R% of mirrors has to be adjusted to experimental set-up due to optical losses and the position of the detection system. It must be possible to open the wall manually to align the cavities. This is achieved by a wall that can be opened with a small motor suitable for vacuum. The laser beam is led into a tube in which the production-cavity is placed. The wall is located in a vacuum tank in the middle. Figures 20 and 21 in appendix A shows a self designed sketch of this vacuum tank. Behind it there is a second tube which contains the regeneration-cavity. The whole system must be in an ultra high vacuum to achieve the desired quantum physical effects by adapting the wavelength of the needed photon to the de-Broglie-wavelength of WISPs[4]. The wavelength of light in a medium depends on the refractive index n: $\frac{c_{vak}}{c_{med}} = \frac{\lambda_{vak}}{\lambda_{med}} = \frac{n_{med}}{n_{vak}}$.
The refractive index n in a gas is related to the pressure by $n \propto p + 1$ for constant temperature. To get a photon speed close to the vacuum velocity of light and therefore a long enough wavelength of light the pressure for ALPS-IIc should finally be $p < 10^{-6}$mbar. In ALPS-IIa and b this pressure should be reached for review, too. For vacuum generation non vibrating pumps are required. That means that displacement pumps cannot be used. The whole experimental set-up has to be free of vibrations to enable the stability of the cavities and generate a Gaussian beam bunch. Otherwise undesirable transversal modes in an oscillating optical resonator may arise. For this purpose one possibility is to use ion getter pumps. The advantage for ALPS-II would be that a large number of these pumps are still present in the existing vacuum system in the HERA tunnel so that the vacuum system could be taken into operation with little effort. The disadvantage of this kind of pumps is that they may emit light in operating mode. No light must enter the vacuum system, especially in the regeneration cavity respectively in the detection system. Ambient light in the regeneration cavity could pretend a non

[10] amplification of escaping optical power related to incoming optical power

existing WISP or disturb the measurements. It must be verified whether the ion getter pumps produce light, and if so, it must be characterized which wavelengths the emitted light contains and if the intensity can be tolerated for the ALPS-II experiments.

6 Vacuum in ALPS-II

6.1 Vacuum Generation

The gas pressure is defined as force acting on an area of a volume generated by the momentum of the random thermal movement of gas particles. It is also the sum of all partial pressures in the volume. For ideal gases the pressure depends on temperature T and the density of gas particles n in $[m^{-3}]$: $p = n_p \cdot k_B \cdot T \Rightarrow p \propto n_p$.

In principal the method for every vacuum generation is to reduce the density of gas particles in a volume. In vacuum a particle can move a longer distance before colliding with another one. This distance, termed as mean free path length λ_p, depends on the diameter and density of particles and is inversely proportional to the pressure[6]:

$$\lambda_p = \frac{1}{\sqrt{2}\pi n_p (r_{p1} + r_{p2})^2} = \frac{1}{\sqrt{2} n_p \sigma_p} \qquad \lambda_p \propto \frac{1}{p} \propto \frac{1}{n_p} \tag{6.1.1}$$

with:

r_1, r_2 – Radii of the interacting particles
σ_p – Cross-section of interacting particles
n_p – density of gas particles

The factor $\sqrt{2}$ is used under assumption of an ideal gas for a precise assessment. In the case of constant temperature T is $\lambda_p \cdot p$=constant.

There are different ways of removing gas particles from the volume to decrease the pressure and to increase the mean free path. Therefore vacuum pumps use several kinds of technical options suitable to their field of application. The two main types are gas transfer vacuum pumps and entrapment pumps. Gas transfer pumps are again divided into positive displacement pumps and kinetic pumps[7]. Positive displacement pumps provide an additional volume which gets filled with gas and is cyclically isolated from the inlet. It transports the gas from the vacuum chamber to the outlet in that way. For this purpose they enlarge and reduce a volume periodically with the compression of gas, or they displace the particles from the chamber directly[7]. Kinetic pumps impart momentum to the gas being pumped so that the gas is transfered continuously from the inlet of the pump to the outlet[7].

Entrapment pumps capture the gas particles by sorption or condensation on their internal surfaces. For sorption usually a chemical active metal or alloy in the form of a thin film is used. The sorption is achieved by cooling surfaces to a temperature low enough to keep the vapor pressure of the condensate below the desired pressure in the vacuum chamber.

One of the main properties of vacuum pumps is the pumping speed S= $\frac{dV}{dt}$ which depends on the size of the pump, the type of pumped gas, the technical implementation and the

pressure. So each pump can only work in a specific range of pressure. To achieve the lowest possible pressure the combination of different kinds of vacuum pumps is necessary. To evacuate a chamber from atmospheric pressure ($\approx 10^3$mbar) to the ALPS-II pressure of $\approx 10^{-7}$mbar it is required to span about ten magnitudes of pressure. So in ALPS-II are three different types of pumps used to generate the ultra high vacuum: the low and medium vacuum is generated by a rotary vane pump firstly. If this is achieved, a turbomolecular pump can lower the pressure to $\approx 10^{-6}$mbar. Now the ion getter pump can be switched on to achieve a minimal pressure of 10^{-9}mbar.

6.2 Ion Getter Pumps

6.2.1 Construction and Operation

Ion getter pumps belong to the entrapment pumps. They take particles out of the gas by ionize them in an electric field. Now the particles have got an electric charge, become accelerated in the electric field and be implanted in one of the inner surface of the pump space. Getter pumps absorb additionally particles on a thin getter film.

It is composed of a casing, the pumping elements and permanent magnets. A pump element consists of two cathodes and a cylindrical anode. This formation is called "Penning Cell". The number of Penning Cells in an ion getter pump influences the pumping speed[8]. Between the cathodes and anodes an electric field is generated by applying a high voltage of a few kV. Available free electrons, for example produced by ionization because of cosmic rays, get accelerated in this electric field. By action of the Lorentz force in the installed magnetic field, they are forced to move on a spiral trajectory to extend their path length to the positive charged anode. In this way their ionization yield increases. The radius of curvature r_e of the electron path determines the length of the ionization path and can be calculated by treating the Lorentz force and the centripetal force as equivalent:

$$e \cdot v \cdot B = \frac{m_e \cdot v_e^2}{r_e} \Rightarrow r_e = \frac{m_e \cdot v_e}{e \cdot B} \tag{6.2.1}$$

The maximal velocity $v_{e,max}$ of electrons depends on the generated voltage between cathode and anode. For non-relativistic case is:

$$E_{kin} = \frac{1}{2} \cdot m_e \cdot v_e^2 = e \cdot U \Rightarrow v_{e,max} = \sqrt{\frac{2eU}{m_e}} \tag{6.2.2}$$

So the maximal radius $r_{e,max}$ and the length of the ionization path could finally be variated by the voltage U and the magnetic flux density B.

$$U = \frac{r_{e,max}^2 \cdot B^2 \cdot e}{2 \cdot m_e} \tag{6.2.3}$$

For ALPS-II ion getter pumps from the company “Varian’ with a pumping speed S=60 l/s are used. They have a magnetic flux density of B≈2T and voltage operating voltage

of 5,9 kV.
So the maximum radius of spiral electron movement is: $r_{e,max} = \sqrt{\frac{2m_e \cdot U}{B^2 \cdot e}} \approx 1.3 \cdot 10^{-4}$m. Due to the voltage free electrons get accelerated and gain kinetic energy. By inelastic collisions they can hit out electrons from gas atoms. Now the ionized atoms get a positive charge by losing an electron and get attracted by the negative charged cathode. They become accelerated, hit against the cathode surface and are implanted in the material. This effect limits the operational lifetime of ion getter pumps[8]. In this way the ion getter pump removes particles from the gas chamber in addition to the chemical sorption due to its getter films: chemical reactive gas particles can be captured in a thin film of a getter material on a inner surface of the pump. The getter film consists of titan usually.

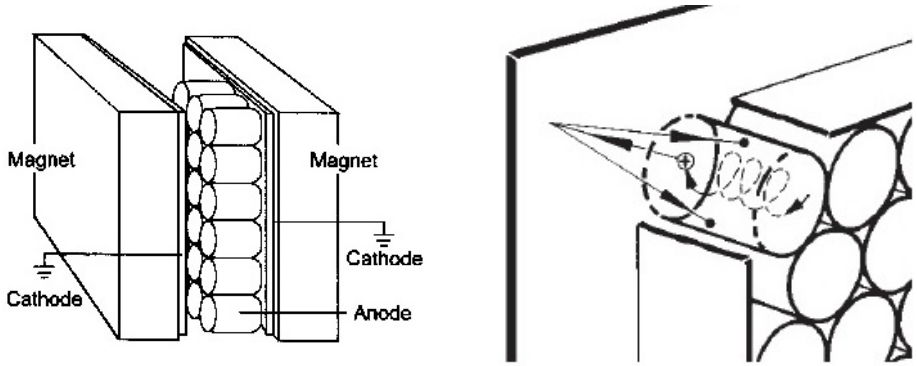

(a) (b)

Figure 2: The principal operation mode of an ion getter pump (a) and the movement of generated ions under the action of magnetic and electric field (b). When ions hit the cathode surface they generate new free electrons as shown[9]

.

Figure 2 shows the operation of an ion getter pump with Penning cells, magnets, anodes and cathodes (a) and the spiral movement of ions in a Penning cell (b) in principal. The movement of the ionized atoms also describe a spiral path. In this case the direction of rotation and linear movement is opposite to that of the electrons. When the ions hit the cathode they produce new available free electrons.

Ion getter pumps are suitable to generate and maintain an ultra high vacuum[11]. They usually should be used with a maximum pressure of p$\approx 10^{-6}$mbar, otherwise the ionization current becomes too high and the voltage breaks down. By baking at temperatures up to T=450° Celsius the inner surfaces of the pump can be cleaned to increase the pumping speed[8].

6.2.2 Ionization of Gases in Penning Cells

There are different possibilities for the ionization of gas atoms: ionization by electron collisions, by ion- and atom collisions (thermally), induced by radiation or indirect ionization. In the pumping room of ion getter pumps mainly electron-impact ionization

[11] ultra high vacuum is defined as the pressure range from 10^{-7}mbar to 10^{-12}mbar

occurs. In ionization electrons transfer kinetic energy to atoms by inelastic collisions: $A + e = A^+ + 2e$. By conservation of momentum and energy an energy-transfer-function can be calculated:

$$\frac{\Delta U}{w_e} = \frac{m_A}{m_A + m_e} \cdot \cos^2 \theta \tag{6.2.4}$$

with:
θ – collision angle of incoming electron an atom
ΔU – modification of internal atom energy
w_e – delivered energy from electron

In elastic collisions electrons only modify the kinetic energy of an atom but not the internal energy U_i. Because of the electric field in the cathode space free electrons get accelerated in an electron cloud. Electrons of this cloud ionize the atoms, if their kinetic energy is sufficient. The created free electrons follow the cloud and so propagation arises. In addition ions generate new free electrons by hitting the cathode to maintain the discharge. Due to this effect current between anode and cathode is flowing. In the workspace of the ion getter pump this current is directly proportional to the gas pressure.

It is only feasible for an electron to kick out a bound electron if its kinetic energy multiplied with the energy-transfer (6.2.4) is higher than the atomic binding energy E_{bin} of this electron. The rise of internal atom energy must be higher than the binding energy of the atom: $\Delta U > E_{bin}$. Therefore exists a minimum value for the voltage, the "breakdown voltage" U_{bd}, that must be generated to produce and maintain the DC-discharge. The U_{bd} is described by Paschens Law (Friedrich Paschen, 1889) for a DC-discharge in a layout with cathode and anode. It depends on pressure, geometry of cathode room (distance between cathode and anode d), temperature and type of gas. To calculate U_{bd} two components are needed: α (first Townsend coefficient) and γ (second Townsend coefficient). α specifies the number of ionizations by an electron on its ionization path length x_0. It is developed from the probability of collision with an atom $P = \frac{x_0}{\lambda_p}$. It follows that α rises if the mean free path length λ_p scales down (or the pressure increases). With knowledge about the ionization cross σ_p of the type of gas can be calculated as well. γ makes a statistical statement about how many free electrons one ion generates by hitting the cathode[10]. For a type of gas the breakdown voltage can be calculated by[11]:

$$U_{bd} = \frac{L \cdot p \cdot x_0 \cdot E_i}{e(ln(L \cdot p \cdot d) - ln(ln(1 + \gamma^{-1})))} \qquad L = \frac{r_A^2 \cdot \pi}{k_B \cdot T} \tag{6.2.5}$$

with:
E_i – ionization energy of the gas $\hat{=}$ binding energy of the electron
r_A – radius of gas atoms
x_0 – ionization path length
α, γ – first and second Townsend coefficient

So the voltage in the ion getter pump should have a suitable value to maintain an ionization. The magnetic flux density can be adjusted to this voltage now.

By the influence of electrons some other effects in the Penning Cells can occur in addition to the ionization: elastic scattering on atoms, dissociation of atoms, recombination of ion and electron and stimulation of atoms. Ionization effects by collision of ion and atom can occur as well.

6.3 Light Emission of Gases

The energy of an electric field, generated by the voltage, would ideally be used only for producing the ionization between the cathodes by inelastic collisions. In reality also some other effects in the cathode room occur. Inelastic collisions without ionizing can take place in a DC-discharge as well. If the kinetic energy of an electron is too low for ionizing an atom, it can stimulate the atom to emit light.

$$A + e \Rightarrow A^* + e \Rightarrow A + e + h \cdot f \tag{6.3.1}$$

with:
A^* – atom in a exited state of energy (a)
$A^* - A = h \cdot f = E_{Photon}$ (b)

The electrons can occupy only defined levels of discrete energies as quantum mechanical states of an atom. Every state has an own value of energy and between them a forbidden place for electrons. Above the binding energy of the most easiest separable electron (ionization energy) there is an energy continuum because the released electrons can move away with any amount of kinetic energy.

The binding energy level of an electron is described by[12]:

$$E_n = -E_R \cdot \frac{Z^2}{n_q^2} \qquad E_R = 13,6eV \tag{6.3.2}$$

with:
E_R – Rydberg energy
n_q – integer main quantum number, which specifies the electron shell
Z – atomic number

If atoms become stimulated but not ionized, electrons can reach a higher energy level E_n in an atom. Atoms want to take the lowest energy state. Therefore the stimulated electrons stay just a short time at a higher energy level, before returning to their allowed ground state E_1. They lose their absorbed energy in this process and emit a photon with $E_{Ph} = E_n - E_1 = h \cdot f$. The energy E_{Ph} is exactly the difference between E_n and E_1 and depends on the specific type of gas. Atoms of each element have different levels of energy so that they are able to emit several different wavelengths.

Furthermore molecules in the rest gas are present. Additionally to conventional stimulation of electrons they can be exited to a vibration or rotation states. This can also be triggered optically by Raman scattering[12] of created photons[13]. The Raman effect describes how photons transmit energy to molecules when they are scattered (inelastic collisions) and change their wavelengths. But the mean free path length λ_{Ph} of photons in a gas is much higher that the free path length of electrons λ_e in the same gas, because the cross section of photons is much smaller than that of electrons in a the gas. The mean free path length of electrons and photons[14] can be calculated similar to the free path length of particles in an ideal gas (see in 6.1.1):

$$\lambda_e \approx \frac{1}{n_p \cdot \sigma_e} \quad \text{and} \quad \lambda_{Ph} \approx \frac{1}{n_p \cdot \sigma_{Ph}} \tag{6.3.3}$$

with:
$\sigma_e \gg \sigma_{Ph} \rightarrow \lambda_{Ph} \gg \lambda_e$
n_p – density of gas particles

Energy levels of oscillations and rotations are intermediate states which subdivide the energy levels of electrons. Because of this molecules also emit lower energetic photons[13] and a larger number of different wavelengths than atoms. The energy of oscillation E_{vib} and rotation E_{rot} can be calculated in the idealized case[13]:

$$E_{vib} = (k + \frac{1}{2})h \cdot f \tag{6.3.4}$$

$$E_{rot} = \frac{h^2}{8\pi^2 I_{mi}} \cdot J(J+1) \tag{6.3.5}$$

with:
f – frequency of the oscillation
k – quantum number of oscillation (integer)
J – quantum number of the rotation (integer)
I_{mi} – molecular moment of inertia

Wavelengths of photons induced by vibration are typically in the middle infrared range and by rotations in the far infrared range[13]. For oscillation various kinds of states are possible: symmetrical and asymmetrical stretching vibrations, swinging vibrations, shear vibrations, torsional vibrations and bob vibrations[14]. These kinds of different states can each be combined and further rotation and oscillation can be combined as well.

So the different atomic gases emit various characteristic wavelengths of light if they are stimulated. For example the possible wavelengths emitted by a hydrogen atom are described by the series of Lyman, Balmer, Paschen, Brackett and Pfund. Because of that

[12] demonstrated experimentally by Chandrasekhara Raman in 1928, postulated by Adolf Smekal in 1923
[13] thereby wider wavelengths

at every gas discharge a visible color can give a statement about the main composition of the portion of ionized atomic gas. The emitted wavelengths of atomic gases are usually short[14]. But due to the molecules in the gas room there could be a various number of more wavelengths, especially longer wavelengths.

6.4 Quadrupole Mass Analyzer

In other words, it is possible to predict the mainly emitted wavelengths of the gas knowing its main components. To determine the components a Quadrupole Mass Analyzer can be used. Its aim is to separate specific elements from the rest gas by using their characteristic mass to charge ratio. This device consists of an ion source to ionize[15] the investigated gas and of four squared and parallel arranged cylindrical rods. Two opposite rods are each connected electrically, and between two rods a voltage which consists of a superposition of DC and AC voltage with frequency ω is supplied:
$U_{sum} = U_a + U_b \cdot \cos(\omega \cdot t)$

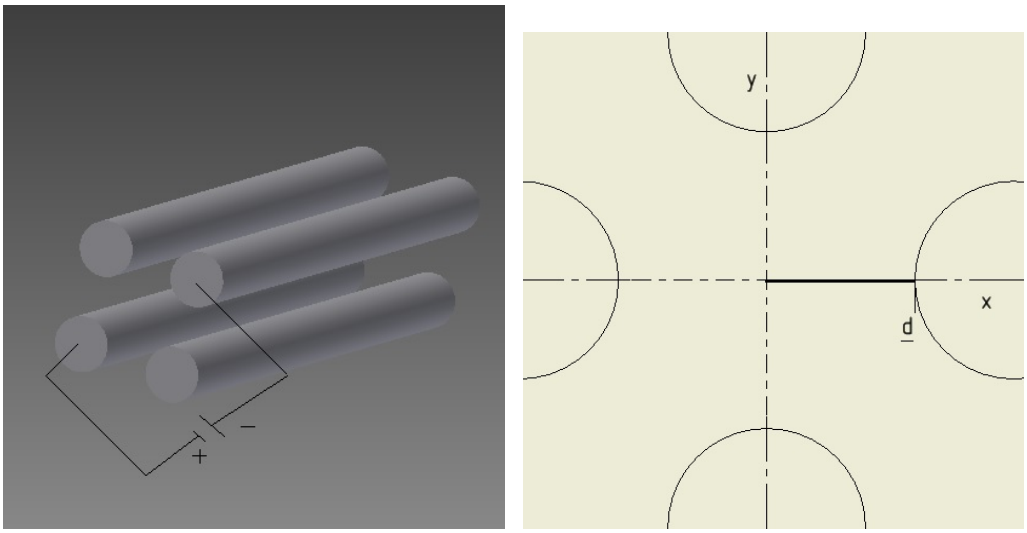

(a) (b)

Figure 3: Four parallel bars of a Quadrupole Mass Analyzer with electrical connectivity (a) and the profile of these four rods with a coordinate system to make mathematical statements for the electric field (b)

Figure 3 shows the four rods of a quadrupole mass analyzer in 3D (a) and the cross section of the rods (b) with the distance d between the center point of the formation and the lateral surface of the bars. The potential of the electrical field between the bars is[15]:

$$\Phi(x, y, t) = \frac{(x^2 + y^2) \cdot (U_a + U_b \cdot \cos(\omega \cdot t))}{2 \cdot d^2} \tag{6.4.1}$$

[14] visible light and shorter wavelengths
[15] for example ionization by electron collision

The electrical field intensity is the gradient of the electrical potential:

$$E_x = -\frac{\partial \Phi}{\partial x} \quad \text{and} \quad E_y = -\frac{\partial \Phi}{\partial y}$$

Hence the absolute value of electrical field intensity is:

$$|E| = \sqrt{E_x^2 + E_y^2} = \frac{U_a + U_b \cdot \cos(\omega \cdot t)}{d^2} \cdot \sqrt{x^2 + y^2} = \frac{U_a + U_b \cdot \cos(\omega \cdot t)}{d^2} \cdot r \qquad (6.4.2)$$

Therefore is E $\propto$ r. Due to this shape of electric field a high frequency AC voltage [16] is supplied to enable to force a charged particle on a spiral path. If the adjusted frequency matches the specific charge to mass ratio of the particle the spiral trajectory is stable so that it can reach a detector. Otherwise it collides with one of the rods and gets behind[15]. The stability of the path is determined by the stability parameter a and b:

$$a = \frac{8qU_a}{\omega^2 d^2 m} \quad \text{and} \quad b = \frac{4qU_b}{\omega^2 d^2 m}$$

The parameters a and b result from solving the "Mathieuschen Differential Equations" [16]. These equations describe the motion of a charged particle and a stable solution means a stable trajectory. As has been shown this stability can be reached by adjusting frequency ω and the voltages U_a and U_b to the mass m and the charge q of a particle. To get a stable solution U_a and U_b have to be adjusted to each other.

By using a quadrupole mass analyzer it is possible to detect and characterize the elements remaining in the rest gas and so to make statements about which wavelengths the ion getter pump may emit basically. This prediction for the purely emitted wavelengths is supplemented by some other effects in the gas room of the pump.

6.5 Continuity Kinds of Wavelengths in the Ion Getter Pump

In addition to the light emission by exited atoms and molecules Synchrotron radiation and Bremsstrahlung can be produced. If the electrons in the cathode room move on spiral paths they lose energy due to the braking in changes of direction. The lost energy is converted into Synchrotron radiation photons with a wavelength which depends on lost kinetic energy of the particle. Furthermore some electrons[17] could crash against any wall of the pump room and emit electromagnetic Bremsstrahlung. Usually X-radiation arises because of these events. For the case of an electron transforming its whole kinetic energy into a photon during one of these events, a minimum possible wavelength of the electromagnetic radiation can be calculated:

$$\lambda_{min} = \frac{h \cdot c}{e \cdot U} \qquad (6.5.1)$$

Following the minimal wavelength of Bremsstrahlung in the used getter pump with U=5,9kV is $\lambda_{min} = 0,21$ nm. That means a photon energy of
$E_{Ph} = h \cdot \frac{c}{\lambda}$=5900eV. All larger wavelengths can be produced above this lowest value so the spectrum is continuous. But the larger the wavelength the rarer is its appearance so that the intensity of photons approaches zero asymptotically.

[16] ω up to 600 MHz
[17] this effects could also be caused by ions in a weaker kind

7 Optical Semiconductor Sensors

7.1 Semiconductors

To detect the light intensity emitted by the getter pump an optical semiconductor is used. Because of their special physical properties semiconductors are materials in experimental physics with a huge number of applications. They have a conductivity between that of metals ($10^3\Omega^{-1}cm^{-1}$) and insulators ($10^{-6}\Omega^{-1}cm^{-1}$) which depends especially on external influences[18]. Semiconductors have weaker electron bindings than insulators, and with the input of energy the electrons become freely movable. Due to this effect the conductivity of a semiconductor or a generated charge quantity can give a feedback signal about the obtained energy input. This can be shown descriptively by a model of band structure[17]:

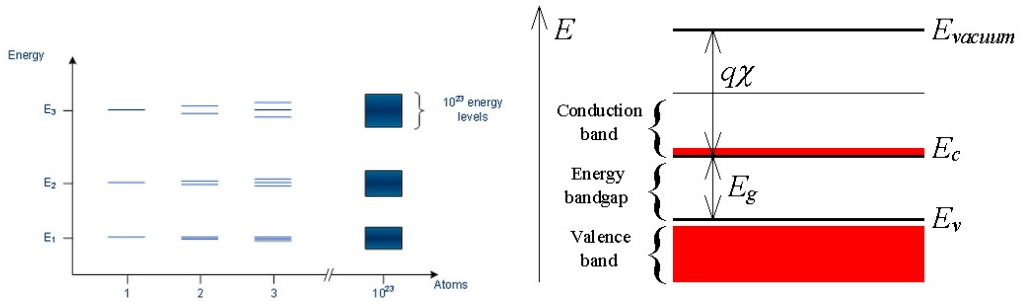

(a) (b)

Figure 4: Discrete energy levels of single electrons form a band (a) and the created energy bands: to lift an electron from the valence band into the conduction band, it must receive an energy $E > E_g$. The difference between E_c and vacuum energy E_{vac} is the electron affinity (needed energy to dislodge an electron from a simply negative loaded ion) $\mathcal{X}$ multiplied by the charge q[18][19]

As described in 6.3 and shown in figure 4 (a), each electron is located in an own discrete energy level. Due to the huge number of electrons in the lattice of a semiconductor and their interactions, these energy levels are intermixed and create broader bands of possible energy states. Between these bands there exists a forbidden area for the value of an electron energy called band gap. E_g is the difference between the highest energy level of the valence band and the lowest level of the conduction band. So an electron has to absorb an energy $E \geq E_g$ to reach the conduction band. If this works, a "hole" remains in the electron lattice. This hole can be regarded as a positive charge carrier.

7.2 Internal Photo Effect of Semiconductors

The density of available charge carriers in a semiconductor rises by increasing the temperature: $n_{cc} \propto e^{-\frac{E_g}{2k_B \cdot T}}$. A different way to supply an electron with energy and to increase the conductivity is optical excitation by irradiating with light. If the wave-

[18] temperature and doping mainly

length of photons is low enough, electrons can jump over the band gap. It necessitates: $\lambda_{Ph} \geq \frac{E_g}{h \cdot c}$. In addition the photon energy has to be lower than the difference between the upper limit of the conduction band and the lower limit of the valence band so that the electron gets placed in the conduction band by laws of quantum physics. The increase of charge carriers is proportional to the intensity of incident light. So the light intensity can be determined by flowing electrical current. It must be taken into account that a semiconductor has a special absorption rate and quantum efficiency[19] QE=$\frac{N_e}{1\ Ph}$ for each wavelength of light.

7.3 Direct and Indirect Semiconductors

Real band gaps look different from the idealized scheme (b) in figure 4. Indeed electrons are matter waves with a wavenumber $k_{ew} = \frac{2\pi}{\lambda_e}$, a momentum $p_{ew} = \hbar k_{ew}$ and an energy $E_{ew} = \frac{\hbar^2}{2m_e} k_{ew}^2$. But this energy is influenced by interaction with other atoms because of the electron arrangement in a lattice. So the bands become deformed and have extreme values for the energy. If minimum of conduction band and maximum of valence band are located on the same value of k_{ew} it is a direct semiconductor. In this case electrons can be stimulated to reach the conduction band by a photon easily. If this extreme values of the bands are situated on different k_{ew} values it is an indirect semiconductor. In addition electrons now have to change their momentum to be excited by a photon in order to reach the conduction band. For this purpose they must obtain a momentum $p_{ew} = \hbar \cdot \Delta k_{ew}$ by interacting with a phonon[20]. Probably one of the most important material in technical usage is silicon, an indirect semiconductor. Silicon has a band gap of E_g=1.1eV so that it can be used as an optical sensor up to an irradiating light wavelength of $\lambda_{max} = 1100nm$.

7.4 CCD-Sensors

These optical properties of semiconductors are used for the operation of “CCD”-elements. CCD is the short name for Charged Coupled Device and was invented in 1970 by Smith and Boyle at the Bell Laboratories in USA. A CCD element is an area of a huge number of pixels arranged like a chessboard. Each of them is normally a MOS[21]- photo diode. In contrast to customary photo diodes, a MOS structure is able to store the charge in a potential well. That means that generated charges not immediately drain away but can be collected over a defined time. The quantity of the generated and stored charge carriers (electron-hole pairs) in the potential well depends on the intensity of incoming light within this period of time, as shown in chapter 7.2. If the irradiating light intensity during the measuring period is too high, electrons can jump over the potential well limit and enter neighboring cells. This effect called “Blooming” induces the overexposure of the CCD camera. Blooming can be avoided with an “Anti-Blooming-gate“ which drains the surplus charges. But with an Anti-Blooming-gate the output signal is no longer linear to the incoming light intensity and so this method is unsuitable for scientific ap-

[19] number of generated electrons N_e by one incoming photon
[20] virtual particle which represents a lattice vibration
[21] Metal Oxide Semiconductor structure

plications. The collected charges are moved little by little after exposure time until the single charge packets reach the read out amplifier[20]. Four square-wave voltages with the same period but different phase relations are superimposed[22]. In this way it is possible to variate the potential well limits and therewith the charge carriers can move between two potential wells. This voltages have high frequencies[23] and generate strong electric fields which cause an electrical read out noise. Figure 5 shows a MOS structure with a potential well for collecting charge carriers and the principle method how this charge carriers are moved to the read out amplifier. Figure23 in appendix A shows the principle of charge carriers transfer of a CCD architecture.

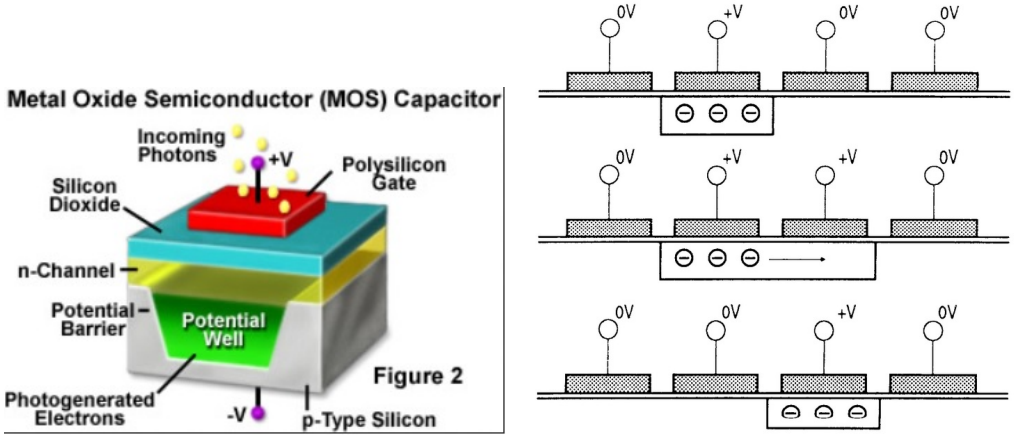

(a) (b)

Figure 5: MOS structure with potential well to store charge carriers in a defined time (a) and principle method to transfer the charge carriers little by little to the read out technology by superimposing square-wave voltages (to increase and decrease the wide range of the potential well)[21][22].

The charge carriers generate a voltage in the amplifier which is read out. This voltage ultimately depends on the light intensity and so the output signal is serial. The MOS structures are linked together by tiny lines and with these the collected charge of each pixel in a defined measurement period can be read out with an Analog-to-Digital converter. The output value of this converter has the unit ADU[24]. With knowledge about the Analog to Digital gain[25] G=$\frac{N_e}{1\ ADU}$ of the specific CCD camera the generated charge quantity can be calculated. Furthermore the quantum efficiency of the CCD chip must be known. With these data the value of ADU can be converted into the number of photons for each pixel. The total number of detected photons in a defined measuring period can also be calculated by summation over the ADU values of each pixel. So the quality of a CCD camera not only depends on the quality of the CCD chip itself but also on the technology to read out, to amplify, and to process the data. At the same time the quality is determined by the offset signal of the camera caused by different effects: dark current, general electrical noise, electrical read out noise, cosmic rays and a

[22] number of superimposed voltages depends on specific CCD camera model
[23] kHz or MHz
[24] Analog to Digital Unit
[25] number of needed electrons to create one ADU

specific read out offset (see 8.2.3). Dark current is a thermal effect which spontaneously generates electrons by heat. To reduce this effect, CCD cameras usually have a built-in cooling system for their chip. The electrical noises cannot be completely reduced, but it is a known systematical offset which is indicated by the manufacturer and can be determined by statistical error calculation. The offsets by cosmic rays are random and can be minimized in the experimental set up.

7.4.1 CCD Cameras "SBIG ST-402ME" and "PIXIS1024B"

In the series of measuring the light intensity in this thesis the CCD Cameras "ST-402ME" by the company "SBIG Astronomical Instruments" and "Pixis" by "Princeton Instruments" are used. Table 2 shows some physical properties of these cameras.

Physical properties	SBIG ST-402ME	PIXIS1024B
chip material	silicon	silicon
maximum detectable wavelength	λ_{max}=1100nm	λ_{max}1100nm
chip matrix	765 · 510 pixels	1024 · 1024 pixels
surface area of the chip	6.9 · 4.3 mm	13.3 · 13.3 mm
surface of one pixel	9 · 9 μm	13 · 13 μm
gain G	2	1
electrical read out noise	13.8 e^-/6.9 ADU	3.85 e^-/3.77 ADU
maximum exposure time t_E	60min	120 min
minimum chip cooling temperature T_{min}	−30°C from ambient	-90°C

Table 2: Properties of the used CCD cameras

Figure 6 shows the quantum efficiency QE of SBIG-402ME and PIXIS1024B each as a function of the wavelength.

With this graphics the QE for $\lambda = 1064$nm is uncertain but was measured by Jan-Eike von Seggern[26] in 2012. It is determined to be QE_{1064nm}=1.2% for both cameras[25].

[26]PhD student at ALPS-II

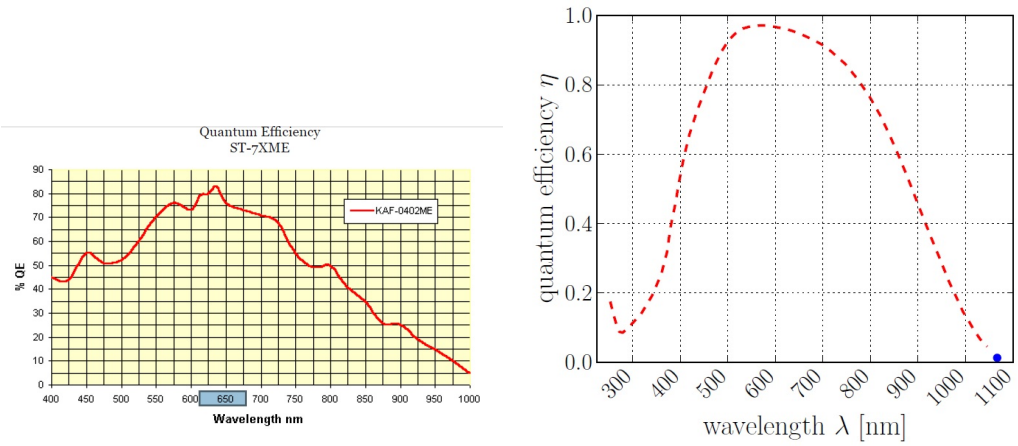

(a) (b)

Figure 6: Quantum efficiency QE (or η) of SBIG-ST402ME (a) and PIXIS1024B (b). The highest sensitivity of SBIG is 83% for a wavelength of 635nm and the highest sensitivity of PIXIS is 95% for $\approx$ 585nm. For a wavelength of λ=1064nm both cameras have a low quantum efficiency of 1.2%[23][24].

8 Measurements and Evaluation

8.1 Residual Gas Analysis of a Vacuum in the Used Pumping Station

An analysis of the residual gas is taken with the mass spectrum analyzer "RGA" by the manufacturer "Stanford Research Systems". The unit in question is a quadrupole mass analyzer. It should only be used at a pressure of p$<10^{-5}$mbar, otherwise the filament, which acts as a hot cathode, gets into danger to rip apart. The pressure is set to p$\approx 2.5 \cdot 10^{-6}$mbar. Figure 7 shows a plot of the mass spectrum.

The gas spectrum has high peaks for the mass numbers 1,2, 17, 18, 28, 44 and further lower peaks for the mass numbers 16, 27, 29 and 41. Table 3 shows the ions which could have these detected mass numbers.

Mass number	Ions	Mass number	Ions
1	H^+	27	$C_2H_3^+$
2	H_2^+, He^{++}	28	$N_2^+, C_2H_4^+, CO^+$
16	O^+, CH_4^+, NH_2^+	29	$C_2H_5^+$
17	OH^+	41	$C_3H_5^+$
18	$H2O^+$	44	$CO_2^+, C_3H_8^+, N_2O^+$

Table 3: Assignment of ions to the mass numbers

The high partial pressure of H_2O is typically for not thoroughly baked out vacuum chambers and is caused by thin water films which arise after aerating. Mass numbers 1 and 2 probably represent atomic and molecular hydrogen. This can be explained by the fact that the turbo molecular pump of the used pumping station has a lower pumping

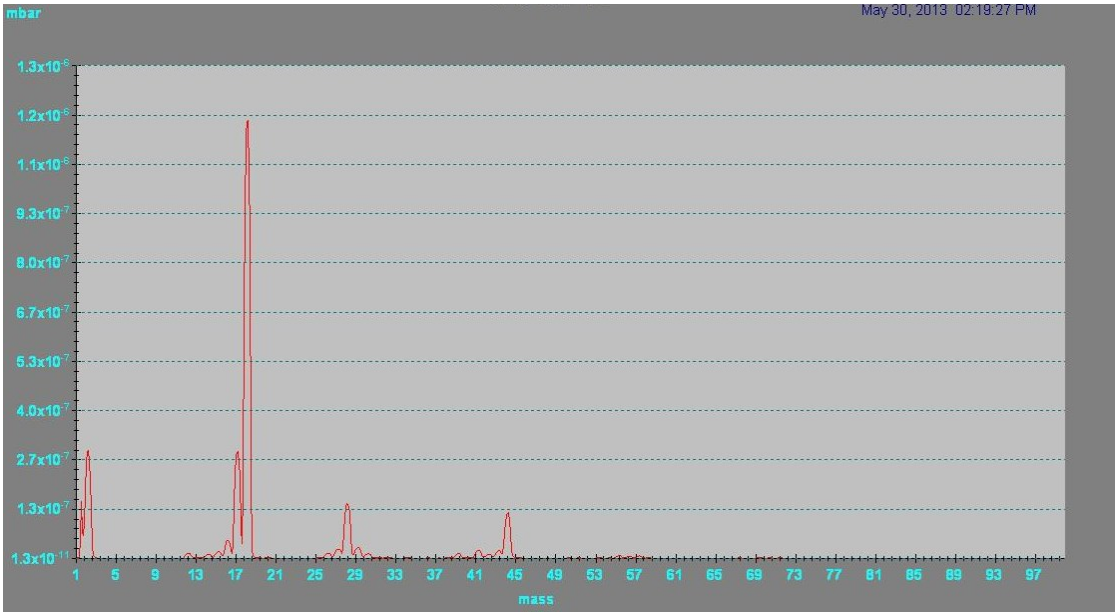

Figure 7: Mass spectrum of the residual particles in the gas at a pressure of p$\approx 2.5 \cdot 10^{-6}$mbar. The spectrum is taken with the mass spectrometer "RGA" by the company "SRS". The x-axis shows the mass numbers of the remaining gas particles and the y-axis their partial pressure

speed for these lightweight particles. The peak of the mass number 28 is possibly caused by a superposition of C_2H_4 and CO ions. The halocarbon compounds of mass numbers 27, 29 and 41 could be caused by lubricants and pump oils. They are clearly visible in the spectrum because of their high ionization probability. Mass number 16 is atomic oxygen or another halocarbon compound. Mass number 28 could be molecular nitrogen or carbon monoxide. Mass number 44 is probably CO_2^+.

The aim of this measurement is not to determinate the exact particle composition of the residual gas but to show that there exist gas particles and molecular particles unison in the residual gas.

8.2 Measurements of the Light Quantity with Optical CCD Sensors

8.2.1 Motivation and Method

So it is really likely that the used ion getter pump emits light, as shown in chapters 6.3 and 6.5. So the aim of the following experimental verifications is to prove how much light it produces. It might be that the emitted intensity of light with a wavelength of λ=1064nm, which is most undesirable for the ALPS-II experiment, is so low that it can be tolerated. For each measurement of light intensity an optical CCD sensor is used. As shown in chapter 7.4 it is possible to detect the produced light quantity with an optical CCD sensor. The principally conceived method is to prove the whole produced

light intensity[27] of the ion getter pump at first and secondly to make statements about whether there are parts of infrared wavelengths in the emitted light as well, a longpass wavelength filter should be used. Finally a bandpass filter should be used to discover the possibly produced intensity of light with λ=1064nm which only lets pass through light with this wavelength. With the CCD cameras SBIG-ST402ME and PIXIS1024B the photon rates emitted by the getter pump should each be calculated.

The probability that an emitted photon hits the the glass fiber entry of the Transition-Edge-Sensor is low. So actually it is not necessary that a possibly existing rate of emitted photons with λ=1064nm is lower than the resolving power of the TES (see chapter 5). Nevertheless the emitted photon rate must not be so high that it becomes a risk to the reliability of the ALPS-II experimental results.

8.2.2 Principal Set Up of Measurements

The ion getter pump has got two openings for the vacuum connections. One of them is linked to the vacuum pump station which contains the rotation vane- and the turbomolecular pump. A vacuum window[28] is screwed onto the other opening. The CCD camera is mounted by a self-constructed connection on the pump such that the camera aperture is in line with the window. A short tube for stability is stuck onto the window. Between camera aperture and the free end of the tube a stainless steel plate with a small round opening is attached. The opening has a diameter of Ø=1 inch and a female thread to screw in filters or lenses. The connection between window and camera must be absolutely light tight so that the camera can only detect light which exclusively comes out of the pump.

Figure 8 shows the ion getter pump with the mounted window (a) and the CCD camera PIXIS1024B put on the window with a special lightproof adhesive tape. The camera is connected to a computer and can be controlled with a specific software.

Figure 9 shows a sectional drawing of the experimental setup. The distance between steel plate and CCD chip is specific for the used camera.

Figure 24 in appendix A shows a photo of a opened ion getter pump. This type of pumps could be used in ALPS-II. The photo is taken in an exhibition at DESY.

The operation voltage of the getter pump is generated by a power supply. The values of voltage and flowing current between the cathodes are each shown on an analog display. The amount of flowing current can be converted into a value of pressure in the pump space by $I \propto p$ (see appendix A, figure 22). So if the pressure in the pump room is too high, the flowing current becomes too big and a power limiter switches off the pump. Before taking a measurement it is must be proven that the set up is light tight. For this purpose the most simplest way is to place the set up in a room with ambient light, turn off the getter pump and take two measurements: at first a measurement M1 with closed internal camera shutter is taken. In this way the camera only detects electrical noise, cosmic rays and a little bit of light, which gets through the camera casing. In a second measurement M2 the shutter is opened and the camera operates over the same exposure

[27] All emitted wavelengths up to 1100nm
[28] the window is made of borosilicate glass by the company “Schott Jenaer Glas”

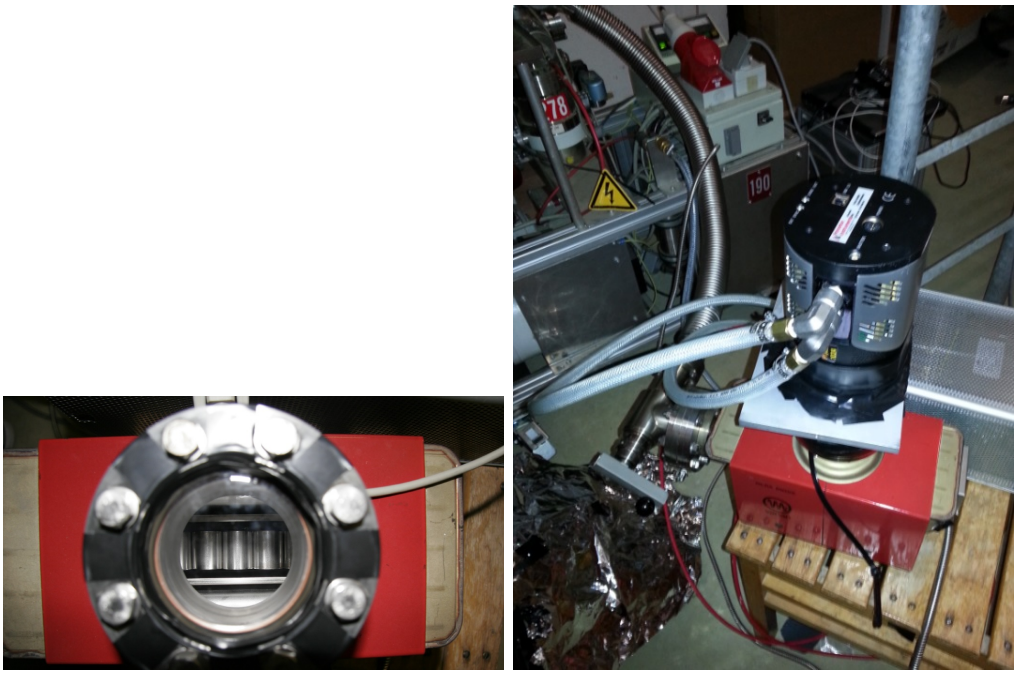

(a) (b)

Figure 8: Ion getter pump with installed vacuum window (a) and the fixed CCD camera PIXIS (b)

time. The difference between M2 and M1 is the detected intensity I_{AL} of ambient light. The Analog-to-Digital converter creates a matrix of values which corresponds with the pixels on the surface of the chip. This matrix can be saved in a computer by using a suitable software. So M1 and M2 are matrices of measured values with the same dimensions and can be subtracted[29]: $M2_{shutter\ open} - M1_{shutter\ closed} = I_{AL}$. After the correction of systematic errors of the measurement (see below in chapter 8.2.3) it must be:

$$\bar{x}_{px}(I_{AL}) = 0 \pm \sigma \qquad \sigma = \frac{s}{\sqrt{n_m}} \tag{8.2.1}$$

with:

$\bar{x}_{px}(I_{AL})$ – mean per pixel of detected ambient light intensity (ADU)
s – standard deviation because of the electrical read out noise
σ_{px} – confidence interval of $\bar{x}_{px}$
n_m – number of measuring values ($\hat{=}$ number of pixels)

The measurement values of these pixels are normally distributed in a "Gauss distribution" . It is possible to calculate a confidence interval for the mean because of the

[29] a measuring value of a pixel is subtracted from the value of the same pixel of the other measurement. For evaluation of all measurements and creation of all graphics the programming language "Python 2.7" is used

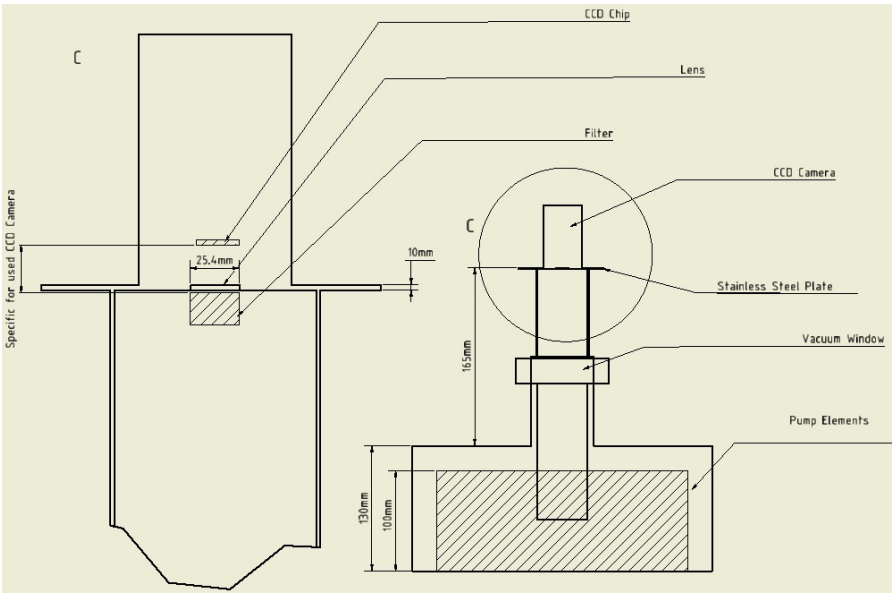

Figure 9: Sectional drawing of the experimental set up

enormous number of measurement values[30] (see below in chapter 8.2.4).

Furthermore one has to notice that the window absorbs a part of the light which shines through. Figure 25 in appendix A shows the transmission of the borosilicate glass. Filters, if they are used, also have a specific absorption spectrum.

8.2.3 Correction of Systematical Measuring Errors

Several errors are unavoidable in measuring a light intensity with a CCD camera as shown in chapter 7.4. The electrical noises can be minimized by subtracting two measurements which are taken with identical measuring conditions. This is the same principal method as in chapter 8.2.2. There are two possibilities to make a subtraction of two measured value matrices M1 and M2:

(a) Shutter remains open for both measurements:

$$M2_{getter\ pump\ on} - M1_{getter\ pump\ off} \tag{8.2.2}$$

(b) Getter pump remains switched on for both measurements:

$$M2_{shutter\ open} - M1_{shutter\ closed} \tag{8.2.3}$$

Both used cameras, SBIG and PIXIS, have another specific systematic error: the detected signal is read out on only one site of the chip and causes an offset on this site. Due to this the specific read out offset is anisotropic and increases with decreasing distance to the read out system. So before correcting the electrical noises (see equation 8.2.2) it is necessary to eliminate this error for each measurement M. For this purpose

[30] $765 \cdot 510 = 390150$ with SBIG and $1024 \cdot 1024 = 1048576$ with PIXIS

it is possible to expand the surface of the chip with two virtual pixel areas by using the software. These both "overscans" extend the chip on two adjacent sides as shown in figure 10 and detect only electrical noise and the specific read out offset. Depending on read out construction the horizontally overscan is placed above or below the physical CCD chip (upright overscan left or right). The following method is applied: for correction in x-direction the mean value of every single column of the horizontally overscan is calculated. Now each calculated mean is subtracted from every pixel value of the same column of the physical CCD chip. For correction in y-direction the same principle is used: the mean of every upright overscan line is subtracted from each pixel value of the same chip line.

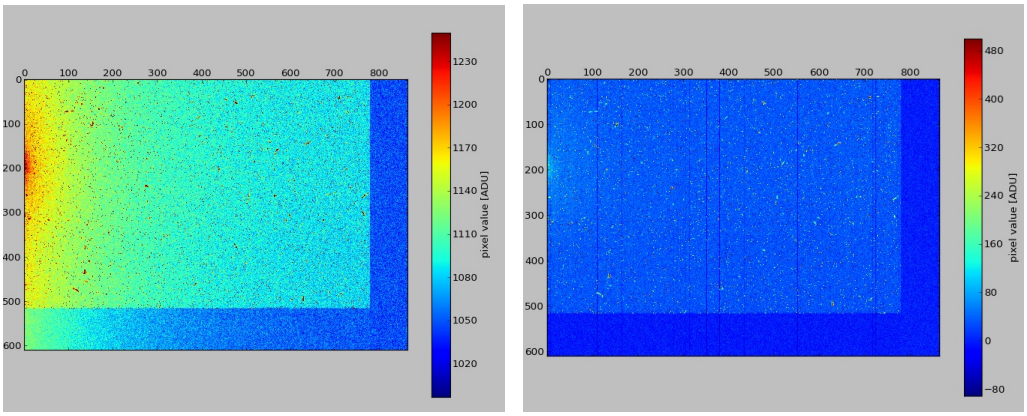

(a) (b)

Figure 10: (a) shows a matrix of CCD chip pixels with overscans for a measurement with closed shutter (unlighted). The stored charges of every MOS structure is read out on the left side. The offset depending on x-direction is clearly visible. By offset correction this offset can be eliminated (b). Both measurements are made by SBIG-ST402ME (Revised and displayed with Python 2.7).

Two pixel matrices are plotted in figure 10. On the right side of each matrix a "colorbar" is displayed, which assigns every ADU-value a specific hue. By the correction of the anisotropic read out offset the general electrical noise is eliminated. This means that only the electrical read out noise due to the read out voltages remains in the physical CCD chip[31]. A few tiny pixel areas (or single pixels) have high ADU values and therefore have a red or yellow shade. This effect arises by cosmic rays. Table 4 shows the mean values of both matrices and the confidence interval for each of them. With these data it is possible to make an estimation about in which magnitude the offsets each are located.

The sum of general electrical noise and specific read out noise is higher than 1000 ADU per pixel in average and does not depend on measuring time. To this fact it is unavoidable to make a detailed error correction to be able to make conclusions to the taken exposures.

After this offset correction the matrix can be cut to the size of the physical CCD chip. The mean values of the overscan areas have to be in the confidence interval of zero now because the mean of every line/column is subtracted from its own pixels. Nevertheless

[31] the overscans are virtual pixels and therefore they are free from electrical read out noises

Value	Matrix a (uncorrected)	Matrix b (corrected)
$\bar{x}_{px}$ (ADU) physical CCD chip	1135.13	60.64
$\bar{x}_{px}$ (ADU) overscans	1048.63	$2.89 \cdot 10^{-6}$
σ_{px} (ADU) physical CCD chip	$\pm$1.04	$\pm$1.03
σ_{px} (ADU) overscans	$\pm$0.14	$\pm$0.13

Table 4: Measurement values before and after correcting specific anisotropic read out offset

it is necessary to rectify errors due to electrical noise (equation 8.2.2) because of the remaining electrical read out noise in the physical chip (mean of $\approx$ 60 ADU, see Table 4).

8.2.4 Measurement Series **A**: Estimated Light Emission of the Ion Getter Pump in General

Firstly it is to prove if the getter pump really emits light. This proof is provided with little effort because it is visible to the unaided eye that the getter pump produces light if it is turned on at the highest possible pressure ($\approx 10^{-6}$mbar) after it has been turned off for a considerable time. Figure 11 shows the luminescence of the getter pump at maximum pressure. The light has a shade of light blue so it is conceivable that mostly blue wavelengths ($420nm \leq \lambda_{blue} \leq 490nm$) are produced[32], but also a wide range of other wavelengths.

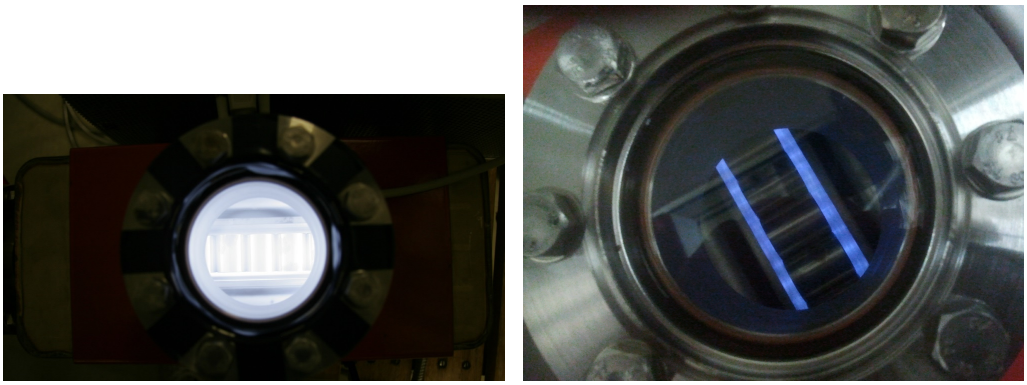

(a) (b)

Figure 11: Light emission of the getter pump at the maximum possible pressure of p$\approx 10^{-6}$mbar straight after switching on (a) and has been running a few minutes (b)

So now it should be proved how high the general emitted light intensity at lower pressure in terms of quality is. Hence several measurement series with SBIG-ST402ME are made. For this series no filter is screwed into the female thread of the plate between vacuum window and camera adaptive. Three measurements A1, A2 and A3 with different exposure times t_E should be exempted of systematical offsets and be evaluated.

[32]this applies to the visible wavelengths of light

CCD camera:	SBIG-ST402ME
Chip temperature:	$-9°C$
Pressure:	$\approx -10^{-9}$mbar
Filter:	no filter

Table 5: Measurement series A: parameters of A1, A2 and A3

Figure 12 shows the histogram for this measurement series.

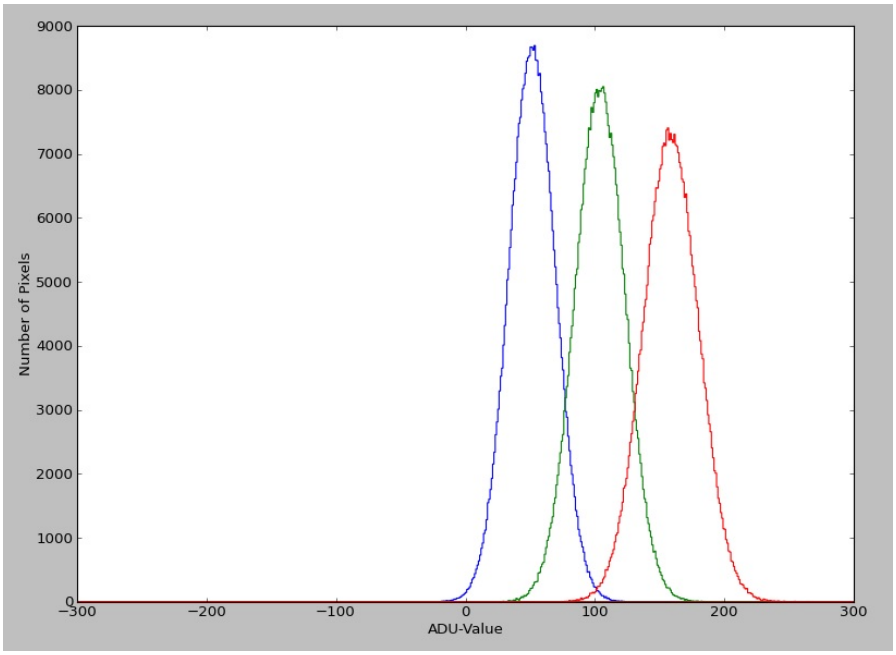

Figure 12: Measurement series A: histogram of measurements A1(blue), A2(green), and A3(red)

The measured values correspond quite accurately to the Gauss distribution because the influences of the electrical noises and cosmic rays are individual random events. The distribution function has the probability density:

$$f(x) = \frac{1}{s\sqrt{2\pi}} \cdot e^{-\frac{1}{2}\cdot(\frac{x-\bar{x}_{px}}{s})^2} \qquad -\infty < x < \infty \tag{8.2.4}$$

with:

$\bar{x}_{px}$	–	mean in ADU, averaged over all pixels
s	–	standard deviation in ADU
x	–	measuring value in ADU

On the assumption that the values describe an ideal Gauss distribution, the mean $\bar{x}_{px}$ matches the ADU-"peak value" of the probability density. The standard deviation s is

defined by: $\bar{x}_{px} \pm s$ contains more than 68.27% of all measuring values x. The standard deviation of each measurement is composed of the specific electrical read out noise of the camera (given by manufacturer, see Table 2) and the other error influences during the exposure, mainly cosmic rays.

Table 6 shows the results of measurements series A.

M	t_E (s)	$\bar{x}_{px}$ (ADU)	s (ADU)	σ_{px} (ADU)
A1	300	51.51	18.56	±0.03
A2	600	104.10	23.99	±0.04
A3	900	158.83	27.56	±0.04

Table 6: Measurement series A: results

$\bar{x}_{px}$ has to increase linear to exposure time t_E theoretically[33]. In this series it almost does, and this fact provides the reliability of the measurements. For a longer measuring time, the peak of the histogram becomes lower. That means that a fewer number of measured values match $\bar{x}_{px}$. Consequently the standard deviation and the confidence interval become larger. This effect is caused by the influence of cosmic rays. The longer the measuring time the more cosmic rays are able to hit the CCD chip. Furthermore negative ADU values are recognizable in figure 12. This bases on the offset correction method: if an unexposed dark frame measurement is subtracted from an exposed measurement, some negative values can come up.

With the results of the measurement series A it is theoretically possible to find out the number of photons N_{ph} which is detected by the CCD chip in the exposure time t_E, and therefore the detected photon rate R_{ch}.

$$R_{ch} = \frac{N_{ph}}{t_E \cdot T_w} = N_{px} \cdot \bar{x}_{px} \cdot \frac{G}{\bar{QE} \cdot t_E \cdot \bar{T}w} \tag{8.2.5}$$

with:

- R_{ch} – photon rate detected by the chip in $\frac{photons}{s}$
- $\bar{QE}$ – quantum efficiency of the used camera (mean)
- G – electrical gain of the used camera
- $\bar{x}_{px}$ – mean of pixels in ADU
- N_{px} – number of exposed pixels
- $\bar{T}_w$ – transmission coefficient of the vacuum window (mean)

$\bar{T}_w$ is calculated from 700 wavelength depended transmission coefficients of the window ($T_w(\lambda = 400nm)$ - $T_w(\lambda = 1100nm)$), which are listed in tabular form in a manufacturer data sheet[26]. So it results in $\boxed{\bar{T}_w \approx 92.3\%}$.

In reality there are two barriers to find out exactly the photon rate R_{gp} which is truly emitted by the getter pump: Firstly it is unknown which wavelengths are emitted by

[33] assuming that the CCD camera is not overexposed

the ion getter pump and what the statistical composition of these wavelengths is like. So a serious statement about the wavelength depending QE can not be given. It is only possible to estimate a value for QE by average over the quantum efficiency of all wavelengths. With manufacturers data sheet (see appendix B, figure 29[23]) it is roughly estimated to $\boxed{\bar{QE}_{all\ \lambda} \approx 55\%}$, assumed that blue wavelengths are represented in the emitted spectrum more often. Secondly only a small share of the whole produced light intensity reaches the CCD chip. The light which passes out of the pump on the connection side must be considered as leakage radiation and not as parallel straight radiation. Therefore it is an estimation to consider the emitted light as a point source and the CCD chip as an area element of the spherical radiation (calculation of the solid angle). The radiation sphere has a surface area of $A_{sp} = 4\pi \cdot r^2$. The radius r corresponds to the distance between pump elements and the CCD chip. For the SBIG-ST402ME this distance is measured to r=212.5mm. Hence it is: $A_{sp} = 2\pi \cdot (212.5mm)^2$. Only the surface of a half sphere is used because it is only relevant how much light the getter pump produces on its connection site. So a rough approximation is to multiply the photon rate R_{ch} by the factor $\frac{A_{sp}}{A_{ch}} = 9562.7$ for a conversion into the photon rate R_{gp} emitted by the getter pump.

As shown it can not be made an exact calculation of how many light the getter pump produces, but it is possible to make a first-order approximation now:

$$R_{ch} \approx \frac{2 \cdot (765 \cdot 510px) \cdot \bar{x}_{px}}{0.55 \cdot t_E \cdot 0.923} \qquad R_{gp} \approx \frac{A_{sp}}{A_{ch}} \cdot R_{ch} \tag{8.2.6}$$

It results in:

M	$R_{ch} \pm \sigma$ in $\frac{photons}{s}$	$R_{gp} \pm \sigma$ in $\frac{photons}{s}$	
A1	$2.64 \cdot 10^5 \pm 154$	$2.52 \cdot 10^9 \pm 1.47 \cdot 10^6$	$\bar{R}_{ch} \approx 2.67 \cdot 10^5 \pm 108$
A2	$2.67 \cdot 10^5 \pm 102$	$2.55 \cdot 10^9 \pm 9.75 \cdot 10^5$	$\bar{R}_{gp} \approx 2.55 \cdot 10^9 \pm 1.03 \cdot 10^6$
A3	$2.71 \cdot 10^5 \pm 68$	$2.59 \cdot 10^9 \pm 6.50 \cdot 10^5$	

Table 7: Measurement series A: first order approximations to photon rates R_{ch} detected by the CCD chip of SBIG-ST402ME and R_{gp} emitted by the getter pump

With measurement series A it is clearly proved that the ion getter pump produces light. Moreover it is even possible to estimate in which magnitude the emitted photon rate is. The evaluation results have a large uncertainty factor due to the unknown quantum efficiency for the assorted irradiation of all wavelengths into the chip and the strewing light propagation. Nevertheless the results are quite reliable for an estimation in which magnitude the average emitted photon rate $\bar{R}_{gp}$ is, as the magnitude remains the same in a range for quantum efficiency of $15\% < \bar{QE}_{all\ \lambda} < 100\%$.

The next step is to prove whether the emitted light contains wavelengths in the infrared range.

8.2.5 Measurement Series **B**: Estimated Light Emission of the Ion Getter Pump with Filter RG850

To review the shares of infrared wavelengths in the emitted light of the ion getter pump a filter "RG850" is screwed into the female thread of the stainless steel plate between camera adaptive and vacuum window. The filter RG850 is a longpass filter, which only lets wavelengths with $\lambda \geq 850$nm pass through. Figure 26 in appendix A shows the transmission curve of the filter RG850[27].

Several measuring series with SBIG-ST402ME are taken. Three measurements B1, B2 and B3 should be shown and evaluated now (similar to evaluation of measurements series A). These measurements should also serve to characterize the emitted light in terms of quality.

CCD camera:	SBIG-ST402ME
Chip temperature:	$-9°$C
Pressure:	$\approx 10^{-9}$mbar
Filter:	RG850 longpass

Table 8: Measurement series B: parameters of B1, B2 and B3

Table 9 shows the results of these measurements.

M	t_E (s)	$\bar{x}_{px}$ (ADU)	s (ADU)	σ_{px} (ADU)
B1	900	3.26	26.79	$\pm$0.04
B2	1800	6.13	33.36	$\pm$0.05
B3	3600	12.27	40.94	$\pm$0.07

Table 9: Measurement series B: results

The mean $\bar{x}_{px}$ also increases almost linear with measuring time t_E (compare to chapter 8.2.4). In this measurement series the statistical composition of each wavelength is unknown as well. To calculate the photon rate $R_{ch,if}$ approximately, a quantum efficiency should be estimated also. For this purpose the mean $\bar{QE}_{\lambda>850nm}$ of the quantum efficiencies of 51 different wavelengths between 850nm$\leq \lambda \leq$ 1100nm should be calculated and used as an estimated quantum efficiency[34]. This approximation can be made more exactly than in chapter 8.2.4 because the range of wavelengths is smaller. It is: $\boxed{\bar{QE}_{\lambda>850nm} \approx 13\%}$.

Furthermore it is required to note the transmission coefficient T_{RG850} of the filter now to calculate $R_{ch,if}$ and $R_{gp,if}$. For this purpose a mean $\bar{T}_{RG850}$ for the transmission coefficient can be determined. $\bar{T}_{RG850}$ is calculated from 26 wavelength depending transmission coefficients of wavelengths between 850nm $\leq \lambda \leq$ 1100nm which are listed in tabular form in a manufacturer data sheet[28]. So it results in $\boxed{\bar{T}_{RG850} \approx 84.8\%}$.

[34] with the hypothesis of a uniform wavelength distribution in the emitted spectrum

For the measurement series B is:

$$R_{ch,if} \approx \frac{2 \cdot (765 \cdot 510px) \cdot \bar{x}_{px}}{0.13 \cdot t_E \cdot 0.923 \cdot 0.848} \qquad R_{gp,if} \approx \frac{A_{sp}}{A_{ch}} \cdot R_{ch,if} \tag{8.2.7}$$

Carrying out this calculation for all measurements results in table 10.

M	$R_{ch,if} \pm \sigma$ in $\frac{photons}{s}$	$R_{gp,if} \pm \sigma$ in $\frac{photons}{s}$	
B1	$2.78 \cdot 10^4 \pm 341$	$2.66 \cdot 10^8 \pm 3.26 \cdot 10^6$	$\bar{R}_{ch,if} \approx 2.67 \cdot 10^4 \pm 234$
B2	$2.61 \cdot 10^4 \pm 213$	$2.50 \cdot 10^8 \pm 2.04 \cdot 10^6$	$\bar{R}_{gp,if} \approx 2.55 \cdot 10^8 \pm 2.24 \cdot 10^6$
B3	$2.61 \cdot 10^4 \pm 149$	$2.50 \cdot 10^8 \pm 1.42 \cdot 10^6$	

Table 10: Measurement series B: photon rate detected by the CCD chip of SBIG-ST402ME

Each value of $\bar{R}_{ch,if}$ and $\bar{R}_{gp,if}$ amounts one magnitude less than the detected and emitted photon rates without filter. The magnitudes of the results remain the same in a range for the quantum efficiency of: $4\% < \bar{QE}_{\lambda>850nm} < 35\%$. This result agrees with the assumption that the emitted spectrum contains a major part of blue wavelengths.

With measuring series B it is clearly proved that the ion getter pump also emits light with wavelengths in the infrared range. The problem is that still no real precise statements about the emitted photon rates can be made. It is only possible to make approximations for the quantum efficiency of the measurements and therefore about $R_{ch,if}$ and $R_{gp,if}$. The results of measuring series A seem to be more precise because of their lower confidence interval σ for the moment, but this is caused by the longer exposure times for measurements of series B. In fact the results of series B are more reliable because the QE is determinable mathematically more accurate.

So with measurements series A and B it is proven that the getter pump emits light in magnitudes which differ up to thirteen decimal powers from the resolving power of the TES. The next step is to check whether the ion getter pump emits light with a wavelength of λ=1064nm. If this is really the case, the light intensity should be characterized in terms of quantity as accurately as possible.

8.2.6 Measurement Series **C**: Emitted Light with λ=1064nm of the Ion Getter Pump

Precise quantitative evidences about the intensity of light with a wavelength λ=1064nm are important for the ALPS-II experiment. Therefore thorough evaluations of this emitted kind of light is the focus of this thesis. This ambition necessitates to apply accurate experimental methods and to minimize all sources of error. The entering wedge was to get a narrow-band filter which only lets pass through light with λ=1064nm. So the ALPS-II group bought a filter "FL1064" which matches the experimental set up and can be screwed into the steel plate as well. Figure 13 shows the transmission of this bandpass filter. It has a FWHM[35] of 10 ± 2nm.

First exposures with SBIG-ST402ME were taken. During these measurements an occurring error was found. The ascertained means $\bar{x}_{ph}$ distribute around x_{ph}=0 ADU. The

[35] full width half maximum

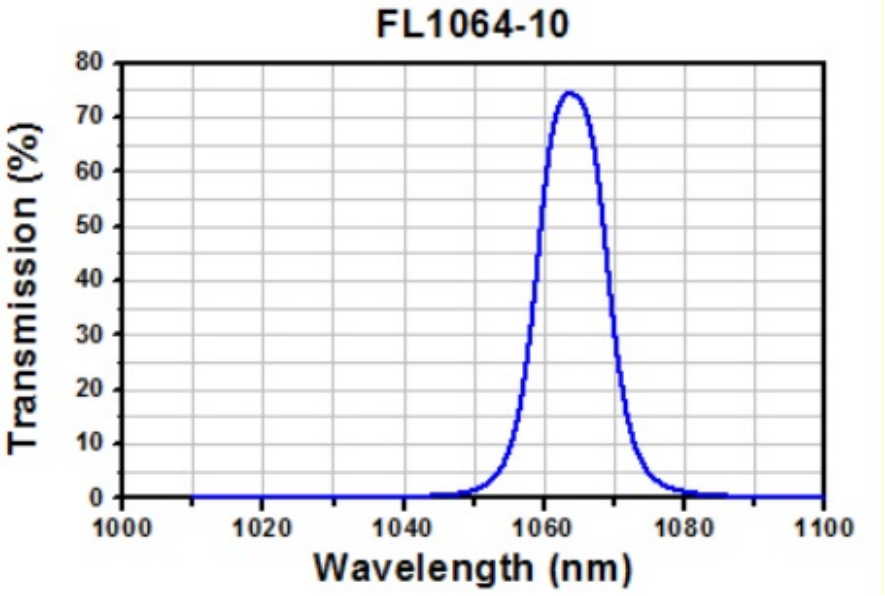

Figure 13: Transmission of the bandpass filter FL1064[29].

values of $\bar{x}_{ph}$ where up to two magnitudes larger than the calculated confidence interval σ of the measurements in this process. Hence it is not possible to conclude with these measurements that the getter pump simply produces no light with λ=1064nm. Table 11 shows an example of these faulty results.

M	t_E in s	$\bar{x}_{ph}$ in ADU	σ in ADU
C1	1800	-1.25	0.028
C2	900	4.95	0.028

Table 11: Measurement series C: faulty results of measurements with SBIG-ST402ME at a pressure of p$\approx 10^{-9} mbar$

The reason for the experimental source of these errors is still unknown despite the efforts to spot the problem[36]. To continue the experimental investigations, the CCD camera PIXIS was used in succession for measuring series C. For this purpose it was only necessary to unfix the SBIG from the steel plate and replace it by the PIXIS. After connecting the PIXIS lightproof to the plate it is possible to use the same experimental set up. This is an important requirement to get comparable experimental results. After the recreation of the experimental conditions the next measurements can be done. The pressure is raised now to increase the light production of the getter pump. This method is justified by the fact that the pressure for the ALPS-II experiment might be up to p=10^{-6}mbar.

[36] measures to find out the source of error: measurements with different detector temperatures, measurements without overscans, measurements at different pressures, measurement with additional light protection for the CCD camera, check of the temperature stability of the CCD chip (in dependence of measuring time and region of the CCD chip

CCD camera:	PIXIS1024B
Chip temperature:	$-50°$C
Pressure:	$\approx 10^{-8}$mbar
Filter:	FL1064 (FWHM=10 $\pm$ 2nm)

Table 12: Measurement series C: parameters of C3 and C4

Table 13 shows the result of a first measurements series with PIXIS and filter FL1064.

M	t_E (s)	$\bar{x}_{px}$ (ADU)	s (ADU)	σ_{px} (ADU)
C3	3600	0.31	40.74	$\pm$0.04
C4	5400	0.91	43.84	$\pm$0.05

Table 13: Measurements C3 and C4

To calculate the photon rates $R_{ch,1064nm}$ and $R_{gp,1064nm}$ it must be considered that the PIXIS1024B has got different technical properties compared to the SBIG-ST402ME. It has a lower gain (G=1), a bigger chip surface, a larger number of pixels on its chip and the exposure times can be set longer. For all subsequent calculations only a narrowed area of the chip ($900 \cdot 950$ pixels) is used because the manufacturers do not guarantee for the reliability of measuring with two marginal small strips. Furthermore the filter has a different transmission compared to the RG850. The filter transmission for a wavelength of λ = 1064nm is $T_{1064,m}$= 75% by manufacturer information[30]. Experimental verifications in the ALPS-II laser laboratory which were supported by Reza Hodajerdi[37], revealed a transmission of $T_{1064,e} \approx 83.1\%$. For calculation of $R_{ch,1064nm}$ it must be considered that the chip surface is $A_{ch} = 950 \cdot 900 \cdot (13.3\mu m)^2$ and the distance between chip and pump elements is r=235mm now. So to find out the photon rate $R_{gp,1064nm}$ emitted by the getter pump, the photon rate $R_{ch,1064nm}$ must be multiplied by the factor $\frac{A_{sp}}{A_{ch}} = \frac{2\pi \cdot (235mm)^2}{950 \cdot 900 \cdot 13\mu m \cdot 13\mu m} = 2401.4$.
The quantum efficiency of the CCD chip is clearly determined at 1.2% for light with λ=1064nm. It has to be:

$$R_{ch,1064nm} = \frac{1 \cdot (950 \cdot 900px) \cdot \bar{x}_{px}}{0.012 \cdot t_E \cdot 0.923 \cdot 0.83} \tag{8.2.8}$$

$$R_{gp,1064nm} \approx \frac{2\pi \cdot (235mm)^2 \cdot R_{ch,1064nm}}{950 \cdot 900 \cdot (13\mu m)^2} \approx 2401.4 \cdot R_{ch,1064nm} \tag{8.2.9}$$

So C3 and C4 demonstrate that the ion getter pump really emits light with a wavelength of λ=1064nm. The photon rates can be calculated quite accurately.

It is remarkable that the photon rates of C3 and C4 deviate from each other (Table 14). The confidence interval increases due to the major number of measuring values.

[37] PHD student at ALPS-II

M	$R_{ch,1064nm}(\frac{ph}{s})$	$R_{gp,1064nm}(\frac{ph}{s})$
C3	$8.01 \cdot 10^3 \pm 1033$	$1.97 \cdot 10^7 \pm 2.48 \cdot 10^6$
C4	$15.67 \cdot 10^3 \pm 861$	$3.76 \cdot 10^7 \pm 2.07 \cdot 10^6$

Table 14: Photon rates of C3 and C4

So the percentage of the confidence interval of $R_{ch,1064nm}$ increases significantly because of the minor amounts of the photon rates. Therefore the uncertainty of the results increases. Despite this effect, the disparity of C3 and C4 can not be considered as a statistical random error because the variation is too large. Due to these results it is to assume that outer influences cause errors during these measurements. One possibility is that the pressure in the getter pump is not constant for both exposure times. An other hypothetical source of error could be the ambient light. For that reason the ion getter pump is separated from the pump station at the anteroom of the laboratory and placed in one of the light-excluded laser laboratories of the ALPS-IIa experiment. So it is excluded that ambient light can influence further measurements and a possible source of error is minimized. The getter pump is pumping itself now without a prevacuum. To achieve more precise results a lens should be used to collect more light, produced by the getter pump. The planned method is to mount a suitable lens in this way that the collected light is focused as effectively as possible on the CCD chip. For that purpose it is necessary to know where the CCD chip is placed in the camera casing (distance between camera adaptive and CCD chip) to adjust the focal length f of the lens to this distance. The distance between camera adaptive and CCD chip is given by the manufacturer[31] and amounts to d_{ch}=30mm. A lens with f_L=25mm is screwed into the female thread in addition to the filter and therewith placed a few millimeters remote to the camera adaptive. With the existing experimental set up it is not possible to determine the distance between lens and CCD chip dead-on but sufficiently accurate.

Now the measurements with filter FL1064 are repeated. The pressure increases once again because the getter pump is not able to reach a pressure which is lower than $7 \cdot 10^{-7}$mbar without connection to the prevacuum pumping station. The chip temperature is ramped down to T=$-60°$.

CCD camera:	PIXIS1024B
Chip temperature:	$-60°$C
Pressure:	$\approx 7 \cdot 10^{-7}$mbar
Filter:	FL1064 (FWHM=10 $\pm$ 2nm)
Lens:	f_L=25mm , Ø=1 inch

Table 15: Measurement series C: parameters of C5

Table 16 shows the results of the modified experimental set up.

By using a lens it is possible to prove clearly that the ion getter pump emits light with a wavelength of λ=1064nm. The detected light intensity increases by three magnitudes compared to measurements C3 and C4. This fact is caused by the increased pressure

M	t_E (s)	$\bar{x}_{px}$ (ADU)	s (ADU)	σ_{px} (ADU)
C5	5400	261.67	145.5	±0.16

Table 16: Measurement C5

of the ion getter pump and the focusing of the light. The standard deviation and the confidence interval increase by one magnitude. To state this fact figure 14 is assistant. It shows the matrix of the measurement C5 (a) and a plot of the means $\bar{x}_{l,m}$ (ADU) of the lines depending on the line number u of the matrix (b). So $\bar{x}_{l,m}$ is representative for measured light intensity.

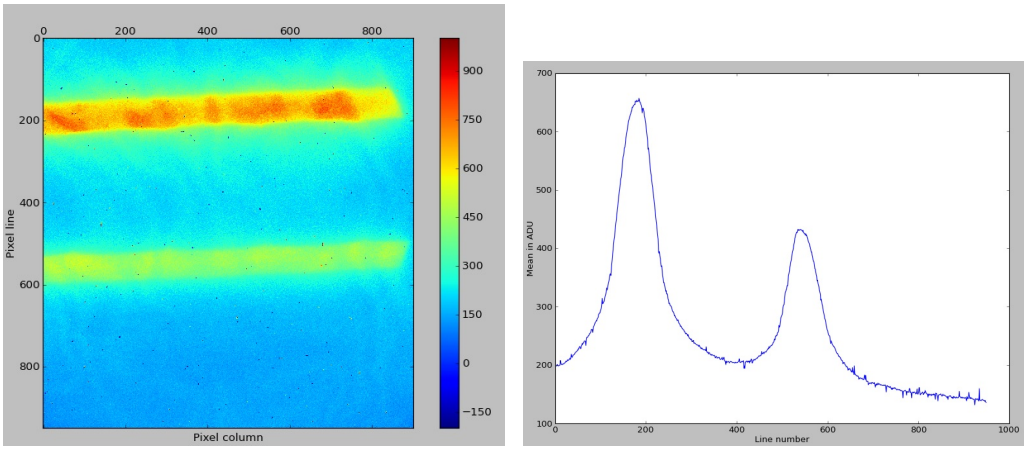

(a) (b)

Figure 14: Measurement C5, Light emission (λ=1064nm) of the getter pump focused with a lens (f_L=25mm): pixel matrix (a) and mean $\bar{x}_{l,m}$ of a line in ADU depending on line number u

.

Figure 14 (a) shows the same structure as figure 11 (b). One of the two illuminating stripes is brighter than the other one, so one can conclude that the lens is adapted skewed. By plotting the means $\bar{x}_{l,n}$ it is recognizable that the two bright stripes create two maximums. The maximums have a pedestal due to the stray light in the pump room. Caused by the skewed adaption of the lens, the pedestal secedes with increasing line number and the left maximum (upper bright stripe in (a)) has a higher peak value of light intensity. To this follows that the standard deviation increases although the detector temperature in measurement C5 is the lowest of all measurements.

In respect of measurement series B and measurements C1-C4 it has been surprising that the ion getter pump produces this high intensity of light with a wavelength of λ=1064nm.

An undesirable property of laser line filters is that they might let pass through small shares of light with half the amount of their defined transmitted wavelength. This effect can be caused by interference effects in the filter medium. The quantum efficiency of PIXIS1024B for light with λ=532nm amounts to $QE_{\lambda=532nm} \approx 95\% \approx 79 \cdot QE_{\lambda=1064nm}$. So if the used filter FL1064 lets pass through light shares with λ=532nm the results

of measurement series C would be useless. For this reason one has to prove if the used FL1064 transmits green light with λ=532nm: the filter is placed between a laser power detector and a laser diode (λ=532nm). Between filter FL1064 and laser diode an additional filter "BG40" is added which only transmits wavelengths $\lambda_{BG40} < 700$nm (see appendix A , figure 27). This is required because the laser diode emits small shares of light with λ=1064nm. To this experiment results that the filter does not transmit green light with λ=532nm. To reach absolute certainty that no green light hits the CCD chip, the line filter was used together with the RG850 filter in further measurements C6 and C7.

CCD camera:	PIXIS1024B
Chip temperature:	$-60°$C
Pressure:	$\approx 7 \cdot 10^{-7}$mbar
Filter:	FL1064 (FWHM=10 $\pm$ 2nm) and RG850
Lens:	f_L=25mm , Ø=1 inch

Table 17: Measurement series C: parameters of C6 and C7

Table 18 shows the results of measurement C6 and C7 with added RG850.

M	t_E (s)	$\bar{x}_{px}$ (ADU)	s (ADU)	σ_{px} (ADU)
C6	5400	235.03	117.11	$\pm$0.13
C7	3600	154..46	82.32	$\pm$0.09

Table 18: Measurement C6 and C7

Figure 15 shows the CCD image of measurement C6 (a) and a plot of the means $\bar{x}_{l,c}$ (ADU) of the column depending on the column number v of the matrix (b). The CCD camera has been rotating 90 degrees by adding the filter RG850.

The detected light intensity decreases compared to C5, caused by the transmission coefficient $T_{RG850,1064mm} = 89\%$ of RG850 [28] for light with λ=1064nm.

To calculate the photon rates it should be noted that the lens does not image the whole light which passes the hole in the steel plate on the chip. This can be caused by its skewed affixing or by the fact that the diameter of the beam is bigger than the CCD chip surface area. By regarding figures 14 (a) and 15 (a) it is recognizable that the imaging of the two bright stripes are tailored on the right side/bottom. Together the cuts have a circular shape which suggests that this tailoring is caused by the edge of the lens. Another option would be that the round shape is caused by the bottom end of the tube, but the bright stripes of the getter pump are too long and the lens is too distant to the bottom end of the tube. So this option is excluded.

Figure 16 shows a plot of the means $\bar{x}_{c,n}$ depending on column number v in C5 (b). It is clearly visible that the intensity of the means have a edge (v$\approx$ 820). For column numbers $v \gtrapprox 820$ the CCD chip only detects stray light of the lens (spherical aberrations). (a) should explain that the ends of both illuminating stripes are caused by the edge of the used lens.

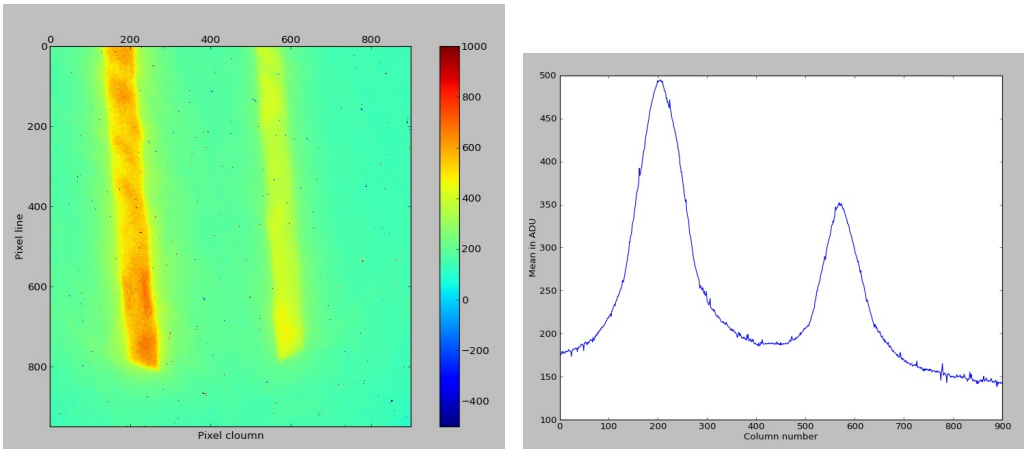

(a) (b)

Figure 15: Measurement C6, Light emission (λ=1064nm) of the getter pump focused with a lens (f=25mm): pixel matrix (a) and mean $\bar{x}_{c,n}$ of a column in ADU depending on column number v (b)

So an approximation must be made about the percentage I_{img} of the light collected by the lens gets imaged on the CCD chip.

It is: $I_{img} = \frac{\text{Area of image on CCD chip}}{\text{Area whole created image}}$.

Furthermore the area element on the radiation hemisphere of the light source is the lens now. The distance r_l amounts to 195mm. To calculate $R_{gp,1064nm}$ this must be considered.

Then the photon rates measured with a lens go to:

$$R_{ch,1064nm} = \frac{1 \cdot (950 \cdot 900px) \cdot \bar{x}_{px}}{0.012 \cdot t_E \cdot 0.923 \cdot 0.83 \cdot T_{RG850,1064nm}} \tag{8.2.10}$$

$$R_{gp,1064nm} \leq \frac{A_{sh}}{A_{lens}} \cdot I_{img} \cdot R_{ch,1064nm} \Rightarrow R_{gp,1064nm} \leq \frac{471.5}{I_{img}} \cdot R_{ch,1064nm} \tag{8.2.11}$$

I_{im}=0.81 by calculation[38]. Due to the inaccuracy of this calculation and the unknown amount of undetected stray light it is useful to calculate a worst case. Because of this a lower limit of I_{img} should be determined. So it should be assumed: $I_{img} \approx 0.75$

With these assumptions the results in Table 19 can be calculated.

The measurements C5, C6 and C7 yield relatively exact repeatable results of $R_{ch,1064nm}$ and $R_{gp,1064nm}$. Thereby C5, C6 and C7 state that the filter FL1064 does not let pass through light with λ=532nm. So the final results are:

$\boxed{\bar{R}_{ch,1064nm} \pm \bar{\sigma}_{ch,1064nm} \approx 4.52 \cdot 10^6 \pm 2.4 \cdot 10^3}$ and $\boxed{\bar{R}_{gp,1064nm} \approx 2.84 \cdot 10^9 \pm 1.27 \cdot 10^6}$.

[38] calculated with the aid of a sketch, which is similar to figure 16

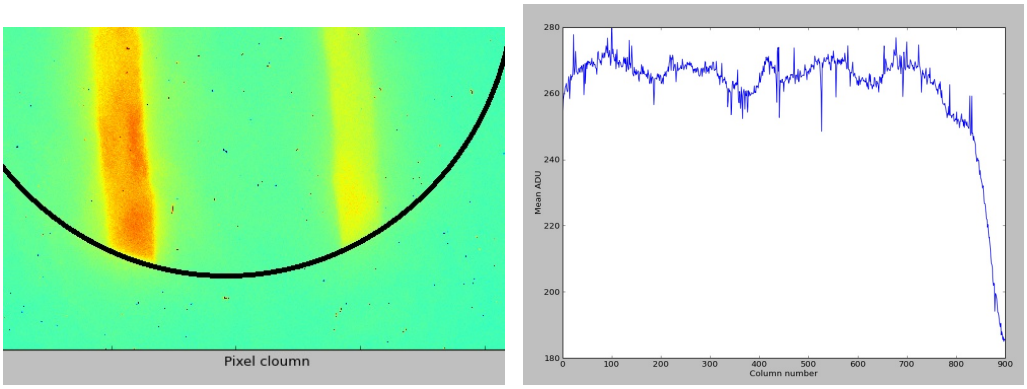

(a) (b)

Figure 16: pixel matrix of C6 with sketched edge of the lens, the bottom of the stripes touch the lens tangentially (a) and mean $\bar{x}_{c,n}$ of a column in ADU depending on column number v

M	maximum $R_{ch,1064nm}(\frac{ph}{s}) \pm \sigma$	maximum $R_{gp,1064nm}(\frac{ph}{s}) \pm \sigma$
C5	$4.51 \cdot 10^6 \pm 2.2 \cdot 10^3$	$2.84 \cdot 10^9 \pm 1.38 \cdot 10^6$
C6	$4.55 \cdot 10^6 \pm 2.5 \cdot 10^3$	$2.86 \cdot 10^9 \pm 1.57 \cdot 10^6$
C7	$4.49 \cdot 10^6 \pm 2.6 \cdot 10^3$	$2.82 \cdot 10^9 \pm 1.63 \cdot 10^6$

Table 19: Photon rates of C5, C6 and C7

These results prove absolutely clearly that the ion getter pump emits a significant intensity of light with λ=1064nm.

Compared to the results of measurements series A and B the photon rates of C5, C6 and C7 have unexpected high values. This is caused by the fact that the results of measurements series A and B without the use of a lens are only rough approximations on the one hand, and that the pressure is two magnitudes higher in measurements C5, C6 and C7 on the other hand: the more particles are available in the penning cells, the more light can be produced. So the light production increases linearly with the pressure in theory. It should be proved experimentally whether this fact can be applied on the ion getter pump.

8.2.7 Measurement Series **D** Light Production of the Ion Getter Pump in Dependence of Pressure

Measurements C5, C6 and C7 result in very high values of the photon rates $R_{ch,1064nm}$ and $R_{gp,1064nm}$ compared to measurements series A and B. Now it should be checked if this can be solely caused by the rise of the pressure. A measurement series D with SBIG-ST402ME is taken: the ion getter pump is connected with the pumping station, but the linking angle valve is closed so that the getter pump is pumping itself. At a pressure of $5 \cdot 10^{-10}$mbar the ion getter pump was switched off for two days, so that the pressure increased to up to $4 \cdot 10^{-9}$mbar. Now the getter pump is turned on and

pumps itself again so that the pressure decreases. Exposures of 1 minute are taken, and between these it is paused for 30 seconds to save the data and start new measurements. The flowing current into the ion getter pump is noted down and can be converted into the value of pressure (appendix A, figure 22). No lens and no filter are used. Before evaluating the measurements are error corrected.

CCD camera:	SBIG-ST402ME
Chip temperature:	$-9°C$
Pressure:	$3.7 \cdot 10^{-9} mbar \geq p \geq 0.8 \cdot 10^{-9}$mbar
Filter:	-
Lens:	-

Table 20: Measurement series D: parameters

Figure 17 shows a plot of average detected light Intensity I_{pre} per pixel in ADU as a function of pressure p in an exposure time of 1 $t_E = 1$ minute.

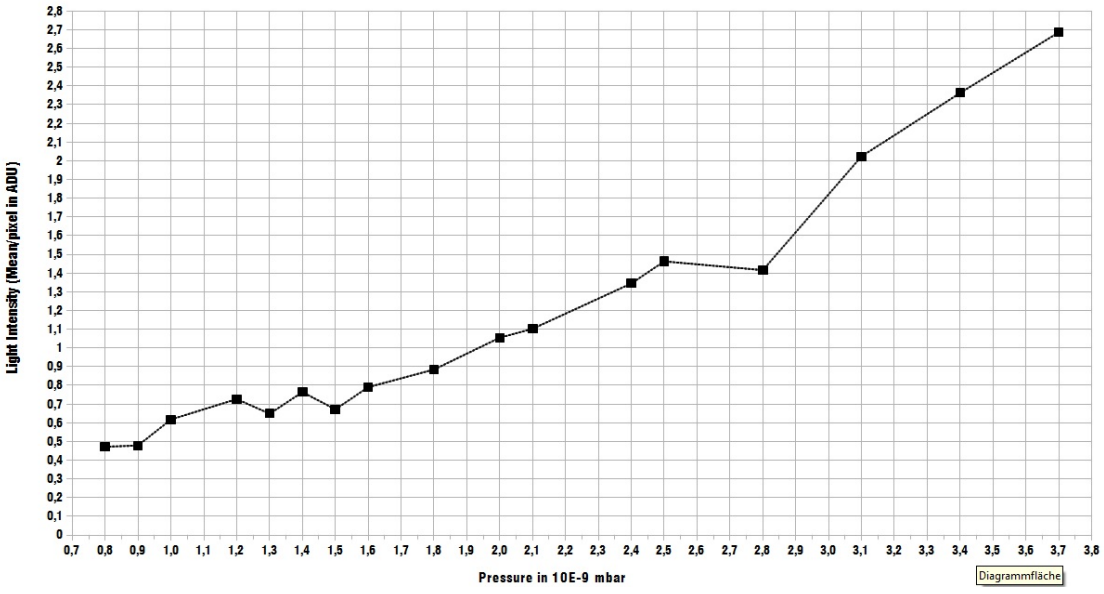

Figure 17: Produced light intensity in an exposure time of 1 minute depending on the pressure in the ion getter pump

The Mean I of detected light intensity per pixel rises linearly with the pressure in the pump room in good approximation. The confidence intervals σ of the single measurements range between 0.027 ADU$\leq \sigma_{px} \leq$ 0.03 ADU, and its mean is $\bar{\sigma} = 0.0273 \approx 0.027$. The result is influenced by a big random error: the analog logarithmic display which shows the flowing current is inaccurate for such small changes of pressure, so that the amounts of flowing current and therefore the pressure is imprecise. Although this error influences the measuring values it can be estimated that the light production increases by one magnitude if the pressure does so.

8.2.8 Measurement Series **E**: Spectral Composition of the Emitted Light

With a measurement series E statements should be made about the spectral constitution of the light emitted by the ion getter pump. For this purpose two filters are available and should be used: the filter RG850 and a second filter BG40. The method is to take a measurement E1 of the whole light intensity emitted by the getter pump without using a filter, and two measurements E2 with RG850 and E3 with BG40. It should be proved approximately, what the ratio of intensity of the two wavelength ranges r_1(300nm $\leq \lambda \leq$ 700nm) and $r_2(\lambda \geq$ 850nm) is like. To achieve this aim the varying quantum efficiencies QE of the PIXIS for r_1 and r_2 must be considered. Furthermore the filters have varying transmission coefficients T. For the average of QE and T estimations $\bar{QE}$ and $\bar{T}$ are made. The mean $\bar{x}_{px}$ (averaged ADU per pixel) is representative for the detected light intensity. The transmission of RG850 and BG40 are shown in appendix A (figures 26 and 27). The parameters of measurement series E are the same as in measurement C5 (Table 15) with the exception of the used filters. First the exposure time without filter is set to t_E=10 minutes. This measurement is useless because the CCD chip is overexposed due to the high pressure and the focusing of the light. So the exposure time has to be reduced to t_E=1 minute lastly so that the getter pump does not get overexposed. The averaged detected light intensity $\bar{I}_{dt}$ (in ADU) by the CCD chip is:

$$\bar{I}_{dt} = \frac{(950 \cdot 900) \cdot \bar{x}_{px}}{\bar{T} \cdot \bar{QE}} \tag{8.2.12}$$

Table 21 shows the results of the measurement series E.

M	Filter	$\bar{T}$	$\bar{QE}$	$\bar{x}_{px}$ (ADU)	σ in ADU	$\bar{I}_{dt}$ in ADU
E0 (t_E=10min)	-	1	≈0.55	overexposed	-	-
E1	-	1	≈0.55	6123.4	6.6	$9.52 \cdot 10^9$
E2	RG850	0.87	≈0.3	797.5	0.7	$2.61 \cdot 10^9$
E3	BG40	0.88	≈0.65	3353.3	2.8	$5.01 \cdot 10^9$

Table 21: Results of measurement series E

With this results it can be calculated approximately, how the wavelengths ranges r_1 and r_2 are distributed by percentage:
$\boxed{\frac{I_{r1}+I_{r2}}{I_{all\lambda}} \approx 80\%}$ and $\boxed{\frac{I_{r2}}{I_{r1}} \approx 52.1\%}$.
The intensities $I(750nm < \lambda <$ 850nm) and $I(\lambda <$ 300nm) together have a percentage of $\boxed{I_{residue} \approx 20\%}$.
Hence the spectrum is approximately composed of
$I_{700nm<\lambda<850nm}$ and $I_{\lambda<300nm}$=20%
$I_{300nm\leq\lambda\leq700nm}$=52.6 %
$I_{\lambda\geq850nm}$=27.4%
Figure 18 shows the exposures of the measurement series E displayed by the software

"WinView". A pixel of the PIXIS becomes overexposed at a detected light intensity of $I_{oe} = 65535ADU$. Figure 18 (a) shows the overexposed measurement E0. The three other graphics show measurements E1 (b), E2(c) and E3(d).

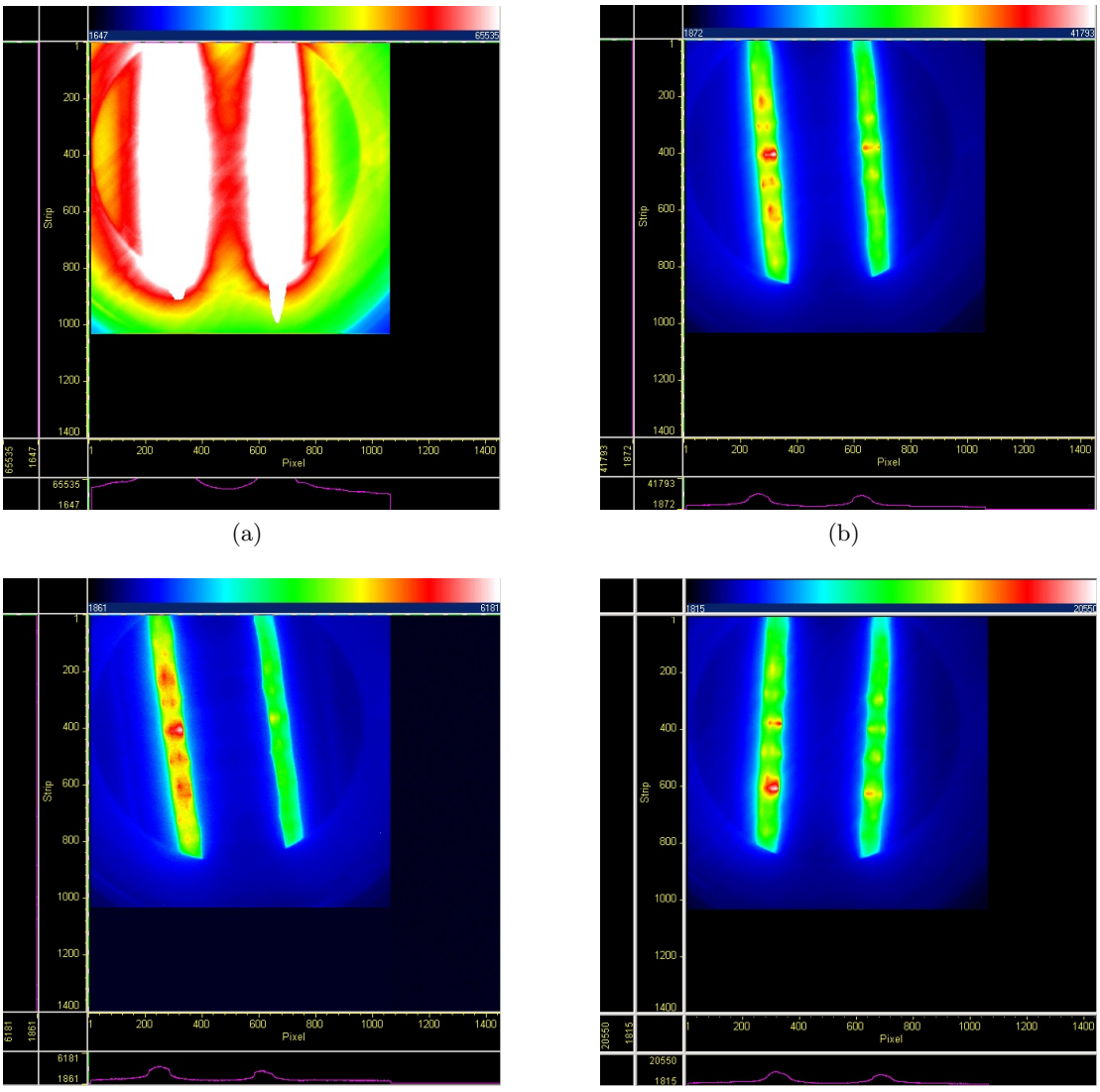

Figure 18: Light emission of the getter pump measured with PIXIS at a pressure of p=$7 \cdot 10^{-7}$mbar and mounted lens (f=25mm): without using a filter (b) and with filters RG850 (c) and BG40 (d)

Figure 28 in appendix A shows two plots: the mean of a column $\bar{x}_{c,v}$ depending on its column number v (a) and the mean of a line $\bar{x}_{l,u}$ depending on its line number u (b). $\bar{x}_{c,u}$ and $\bar{x}_{l,v}$ are representative for the averaged detected light intensity in lines/columns.

9 Summary

The achieved results of the experiments carried out are of great importance for the ALPS-II experiment. Up to now it has been absolutely unclear whether the existing ion getter pumps really emit light with a wavelength of λ=1064nm. It can be assumed that the results of the experiments carried out are unique as literature studies can not give any information concerning this issue. Still it needs to be taken into account that ultimately the results of the experiment can not be considered as absolutely correct. Especially the fact that it can not be determined precisely which percentage of the emitted light really reaches the CCD chip lowers the reliability of the obtained results. Nevertheless, with the conceived experimental set up it is possible to make a reliable statement in which magnitude the emitted photon rates for different ranges of wavelength and light with a wavelength of λ=1064nm are placed. Table 22 again summarizes the most important results of the experimental measurements.

Measurement series	range of detected λ	% of the emitted spectrum
E1	0nm$< \lambda \leq$ 1100nm	100 %
E2	850nm $\leq \lambda \leq$ 1100nm	27.4 %
E3	300nm $\leq \lambda$ 700nm	52.6 %
E1,E2,E3	Residual ranges of λ	20%
Measurement series (p in mbar)	**Range of detected λ**	**R_{gp} in ph/s**
A (10^{-9})	0nm $< \lambda \leq$1100nm	$2.55 \cdot 10^9 \pm 1.03 \cdot 10^6$
B (10^{-9})	850 $\leq \lambda \leq$ 1100nm	$2.55 \cdot 10^8 \pm 2.24 \cdot 10^6$
C5,C6,C7 ($7 \cdot 10^{-7}$)	λ=1064nm	$2.84 \cdot 10^9 \pm 1.27 \cdot 10^6$

Table 22: Summarize of important experimental results

Due to the wavelength depended quantum efficiency of the CCD cameras the reliability of the achieved results depends among others on the composition of the wavelength spectrum of the emitted light. It could be shown that the assumptions for the percentage composition of the spectrum made in measurement series A-C are true with sufficient accuracy. Because of its functional principle in operation the ion getter pump emits light. In this process the intensity of this light is directly proportional to the prevailing pressure in the pump room.

With the obtained results it is clearly proved that the emitted light also includes light with a wavelength of λ=1064nm. There is a great probability that this light is generated by excited molecules in the pump room, which could be proved by means of the residual gas analyzer. The photon rate of light with λ=1064nm emitted by the ion getter pump is higher by 11 magnitudes as the resolving power of the Transition Edge Sensor used in the ALPS-II experiment. The experimental results of measurements C5, C6 and C7 have the biggest reliability compared to measurement series A and B, as the quantum efficiency of the CCD camera for measurements C5-C7 is clearly defined. The results of the measurements are reproducible very well. The fact that the emission rate of photons with λ=1064nm is the highest bases on the high pressure in the pump room in measurements C5-C7.

10 Prospect

With this thesis the initially requirements could be met. Reproducible experimental results could be achieved and realistic approaches for the light emission of the ion getter pump have been provided. As there have not been any further physical publications for the taken measurements of emitted light intensity so far, these measurements should still be repeated another several times for more accuracy and certainty and if possible more precise experimental methods should be developed and applied.

Furthermore the achieved results need to be integrated into the experimental requirements of ALPS-II. It will have to be verified how many of the emitted photons in the set up of the ALPS-II experiment in reality reach the Transition Edge Sensor eventually. With more and more accurate and reliable measurements of the produced photon rate of light with λ=1064nm and the probability of how many of the emitted photons would be detected, a decision will have to be made whether the ion getter pumps can be used for the ALPS-II experiments.

11 Appendix

A Figures

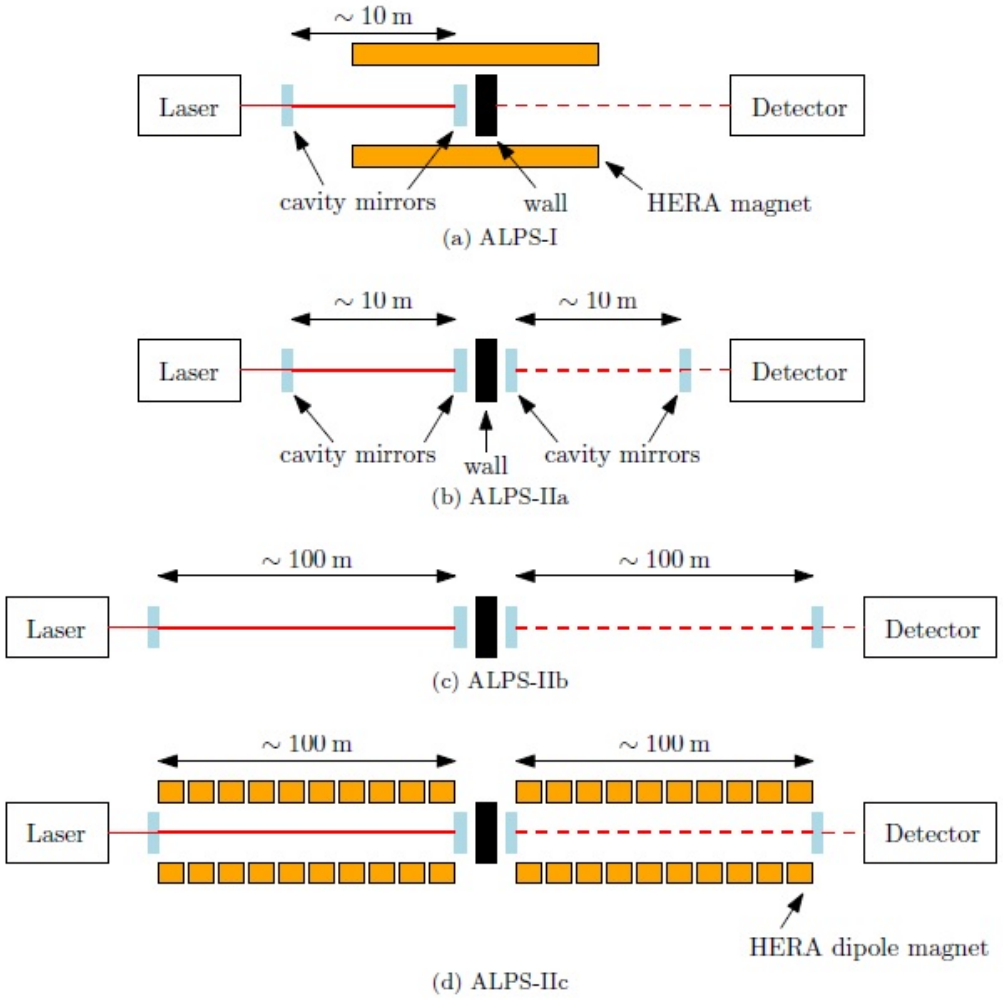

Figure 19: Experimental set ups of ALPS-IIa, ALPS-IIb and ALPSII-c[4]

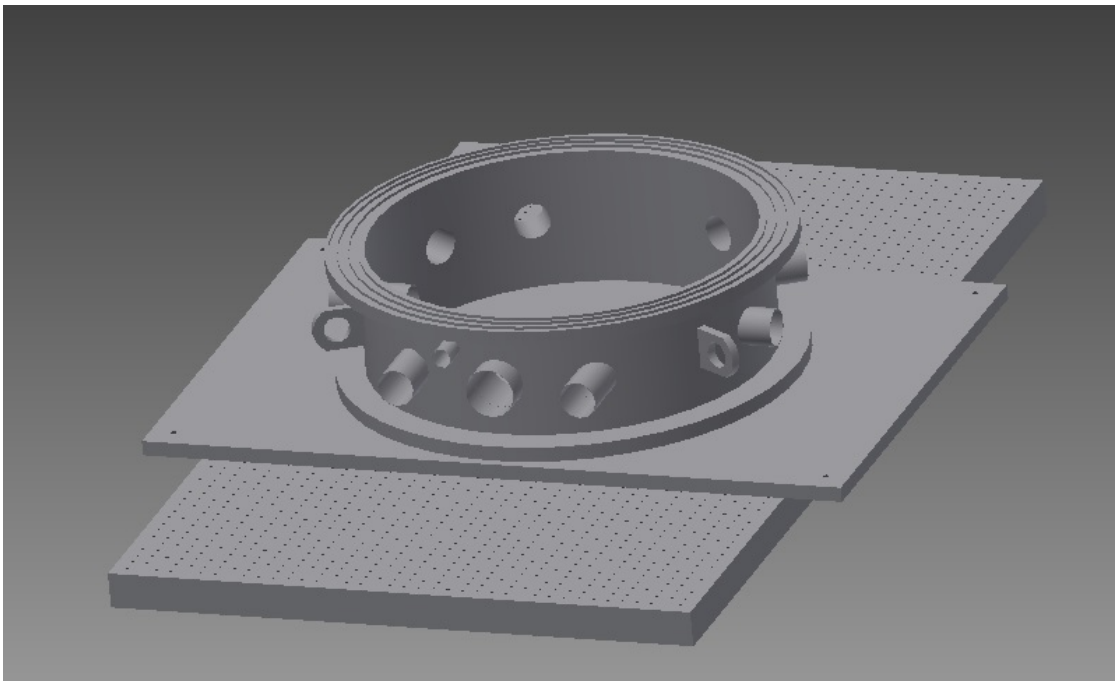

Figure 20: 3D model of the opened vacuum tank (with connections to regeneration cavity, production cavity and detection systems) used in ALPS-IIa, drawn with the software "Inventor 2013"

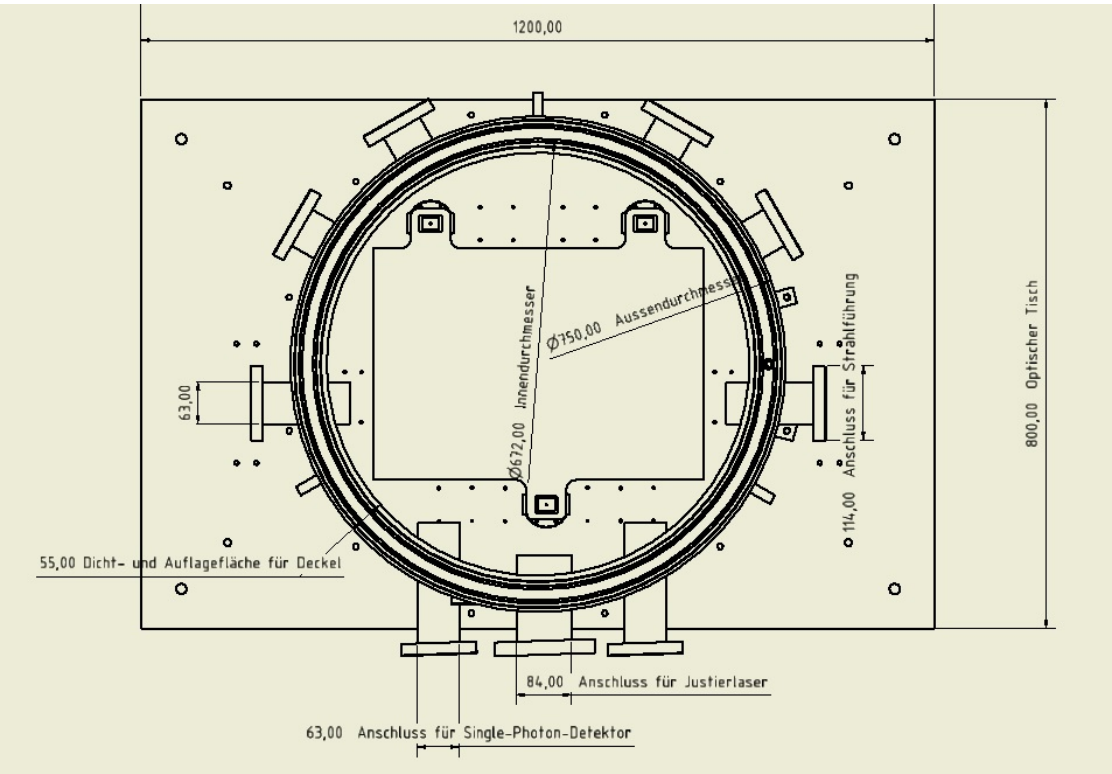

Figure 21: Sectional sketch of the vacuum tank, used in ALPS-IIa, drawn with the software “Inventor 2013”, German inscriptions

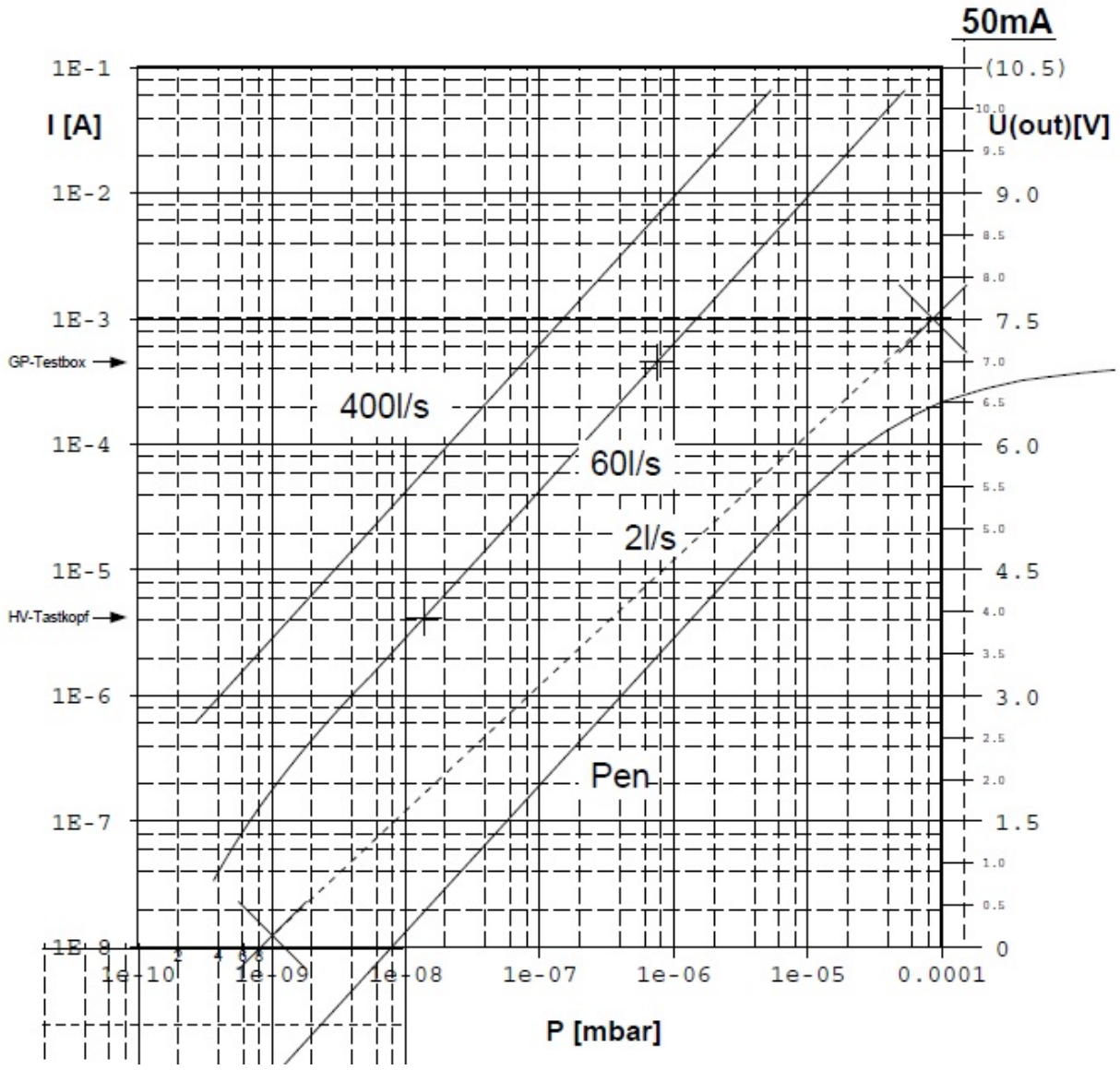

Figure 22: Diagram for the conversion of flowing current of the ion getter pump into pressure. The used getter pump has a pumping speed of 60 l/s[33]

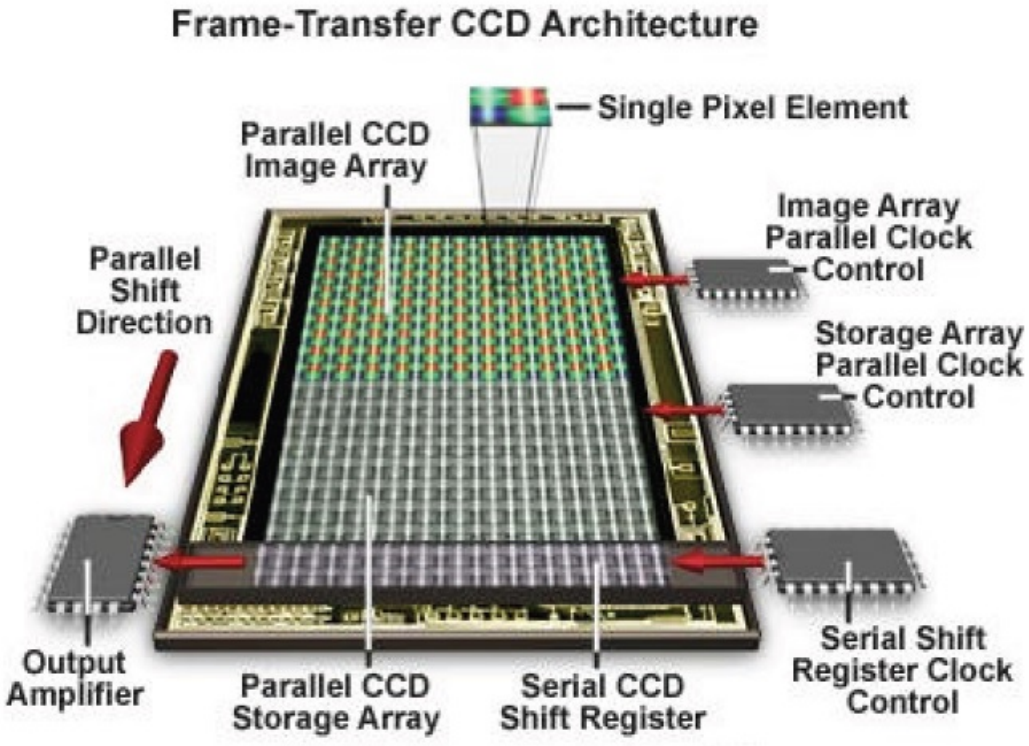

Figure 23: Transfer of generated charge carriers of a CCD chip[34]

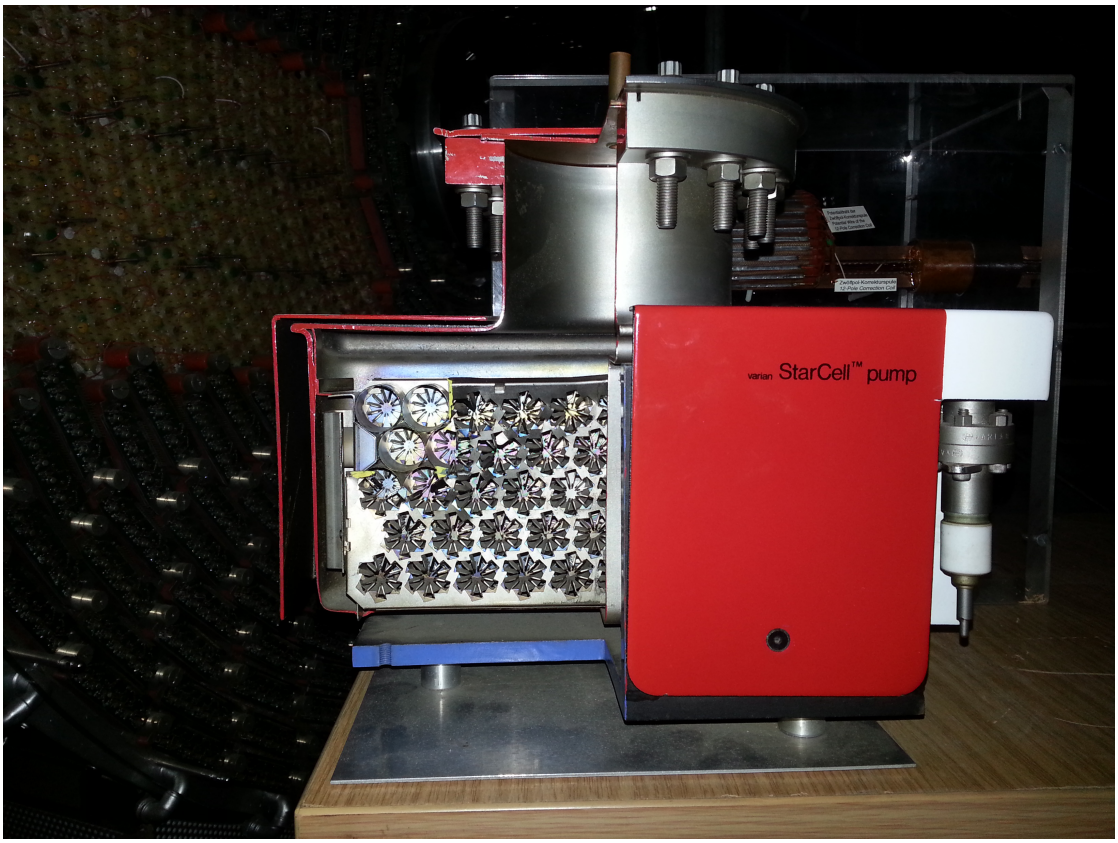

Figure 24: Opened ion getter pump in an exhibition at DESY

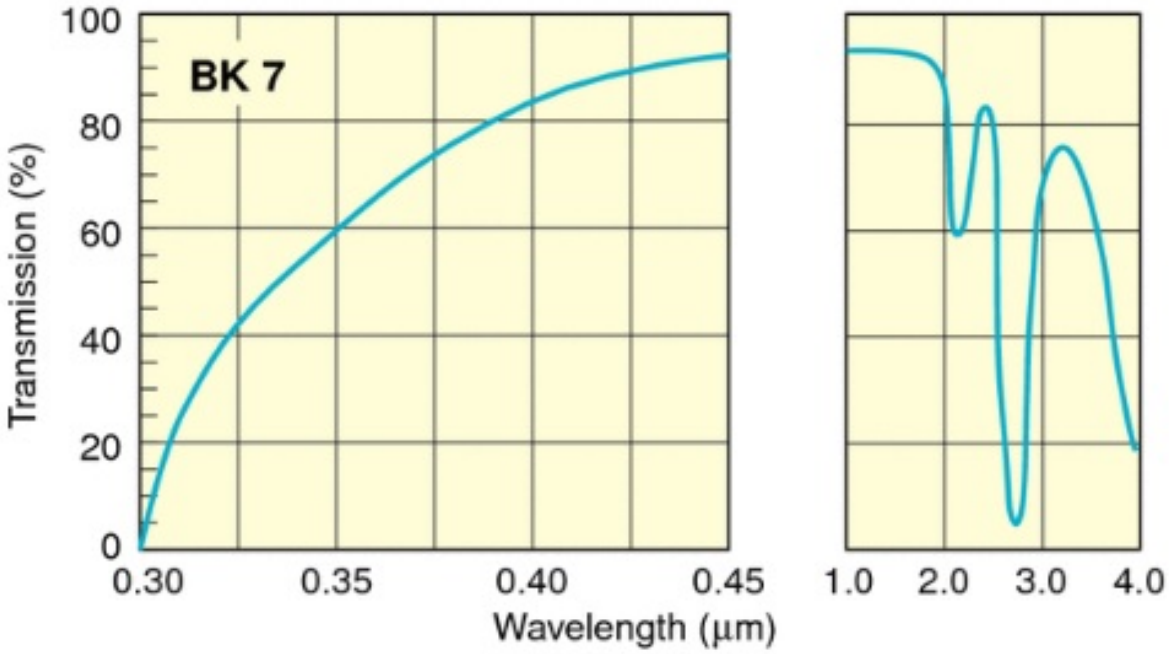

Figure 25: Transmission curve of the borosilicate glass vacuum window[26]

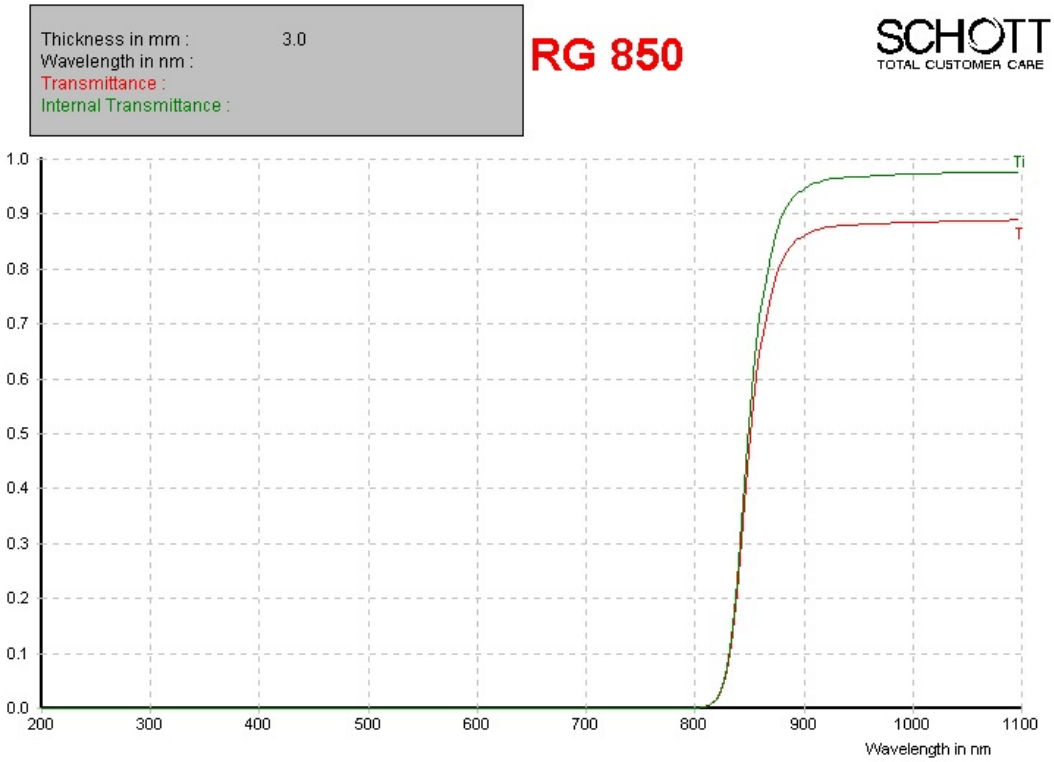

Figure 26: Transmission of the longpass filter RG850[28]

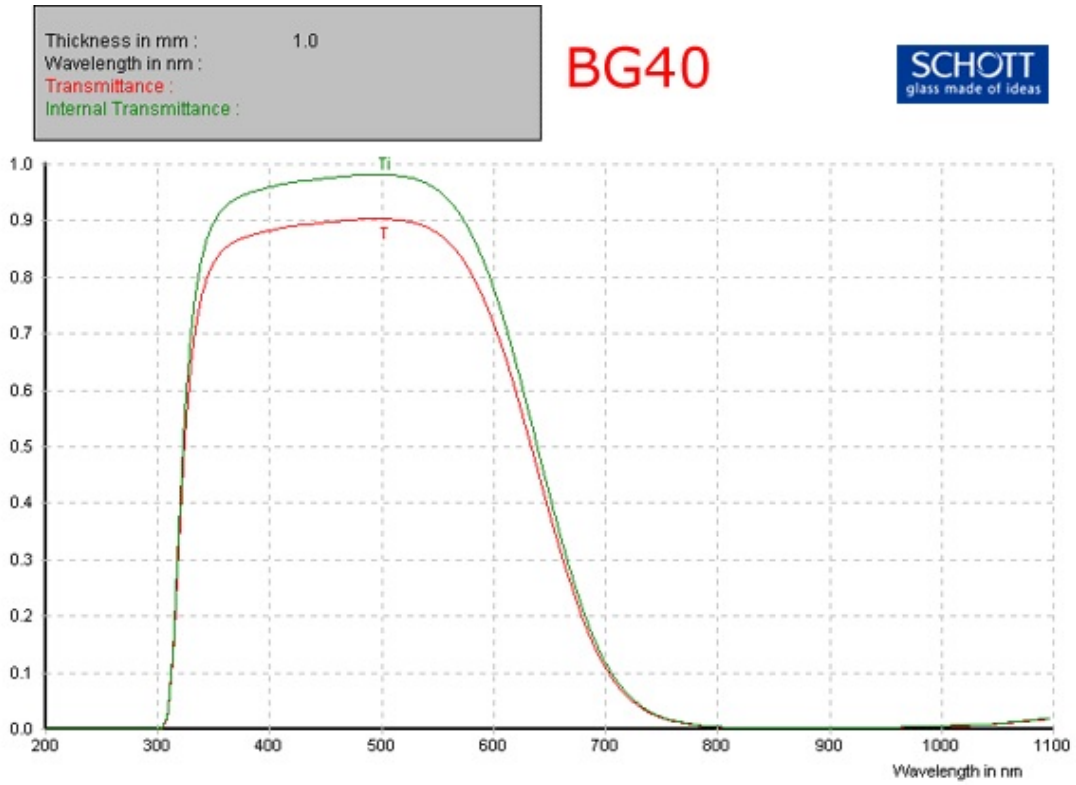

Figure 27: Transmission of the short pass filter BG40 (b) which only lets pass through short wavelengths with $\lambda \leq 700nm$ [32]

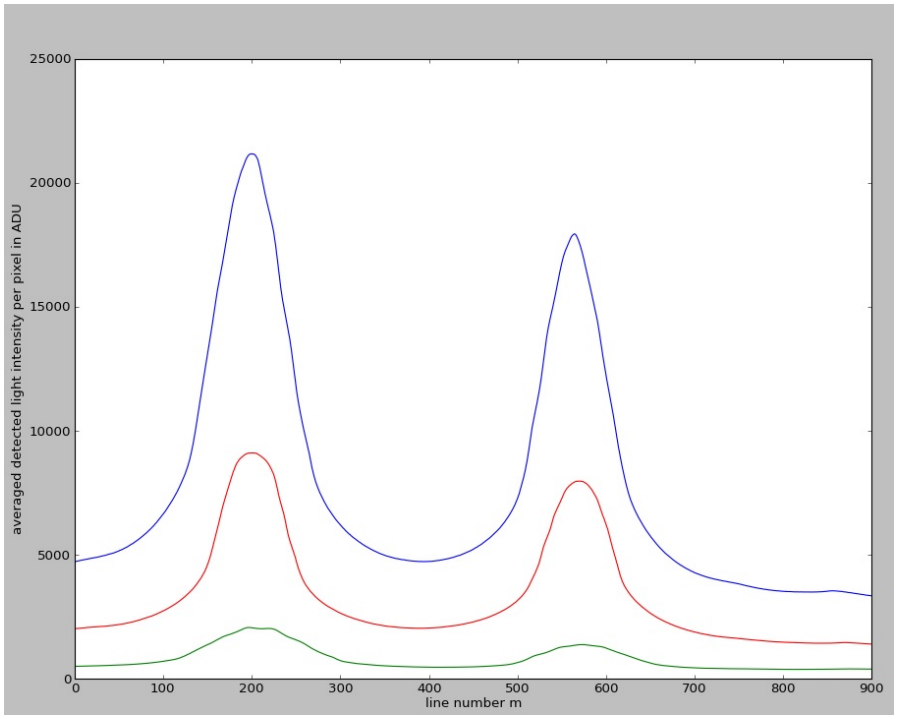

(a)

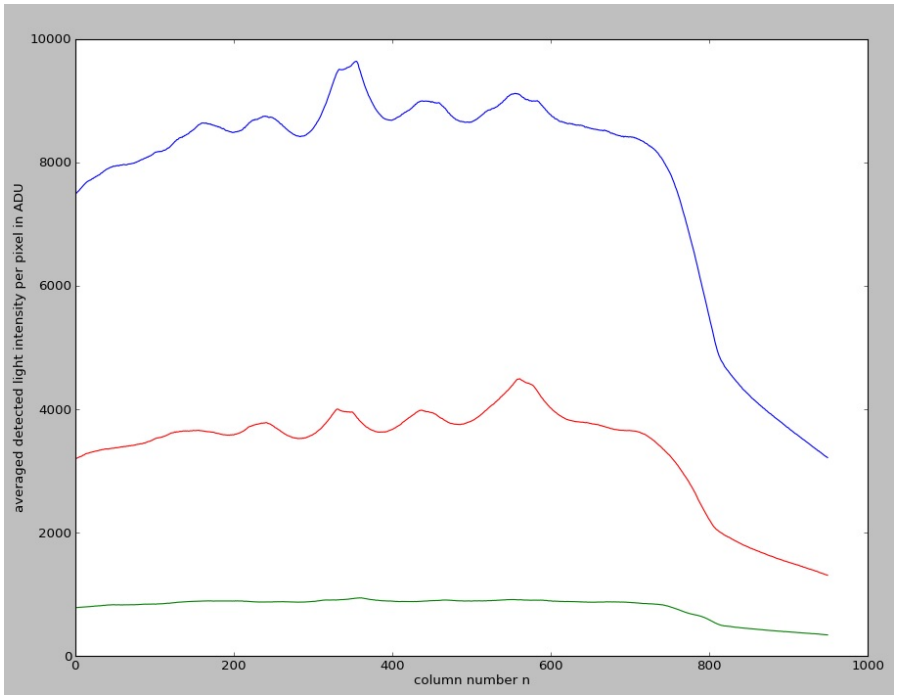

(b)

Figure 28: Averaged detected light intensity per line (a) and column (b) in ADU in dependence of column/line number. For each plot E1 is blue, E2 is green and E3 is displayed red.

B Data sheets

Imaging CCD	Kodak KAF-0402ME
Imaging/Pixel Array	765 x 510 pixels
CCD Size	6.9 x 4.3 mm
Total Pixels	390,000
Pixel Size	9 x 9 microns
Full Well Capacity	~100,000 e-
Dark Current e/p/s at 0 C	1e-/pixel/sec at 0 deg. C
Antiblooming	NABG Only
Peak QE	~85% Peak, ~75% at H-a
Shutter	Electromechanical
Exposure	0.09 to 3600 seconds, 10ms resolution
Correlated Double Sampling	Yes
A/D Converter	16 bits
A/D Gain	1.5e- unbinned, 2.0e- binned 2x2, 3x3
Read Noise	13.8e- RMS Typical
Binning Modes	1 x 1, 2 x 2, 3 x 3
Pixel Digitization Rate	Up to 800k pixels per second with USB 2.0
Full Frame Download	<1 second
Focus Mode	<1 second
Cooling Delta	Single Stage TE, -30C from Ambient
Temperature Regulation	+/- 0.1 deg. C
Power	12VDC, Power Supply Included
Computer Interface	USB 2.0
Computer Compatibility	Windows 32 and 64 bit OS, Mac
Dimensions	5 x 4 x 2.5 inches (including fan)
Mounting	T-Thread,
Weight	Approx. 20 oz. (0.6kg)
Backfocus	0.69 inches (c-mount compatible)
Filter Wheel Option	Internal RGBC or Internal BVIC
Self-Guiding Filter Wheel	n/a
Filter Size	custom
Adaptive Optics Option	n/a
Remote Guide Head	n/a
Lens Adapter	C-mount, Nikon or Canon FD 35mm lens
OAG Option	n/a

Figure 29: SBIG: Data sheet[23]

References

[1] *Planck 2013 results : XVI. Cosmological Parameters, arXiv:1303.5076*

[2] `http://www.astro.uni-bonn.de/~deboer/pdm/pdmdmtxt.html`, reviewed 20.8.2013

[3] `http://www.weltderphysik.de/gebiet/astro/kosmologie/gravitation/gravitationslinsen/`, reviewed 26.8.2013

[4] *ALPS-II : Technical Design Report, 2012,arXiv:1302.5647*

[5] Prof. Dr. Harald Bergner : Lasertechnik, course, Ernst-Abbe-Fachhochschule Jena, 12/13

[6] Prof. Dr. Harald Bergner : Vakuumtechnik, course, Ernst-Abbe-Fachhochschule Jena, 11/12

[7] James M. Lafferty : Foundations of Vacuum Science and Technology, 1998, Canada

[8] *vacom, data sheet*, reviewed 28.8.2013 `http://www.google.de/url?sa=t&rct=j&q=&esrc=s&source=web&cd=2&sqi=2&ved=0CDcQFjAB&url=http%3A%2F%2Fwww.vacom.de%2Fdownloads%2Fvacom-produktkatalog%3Fdownload%3D2307%3Aionengetter-und-titansublimationspumpen&ei=xtAAUumGLMfqswaamoG4Dw&usg=AFQjCNE1OvW2-jkKw5lF8PGn4IokvKjecA&sig2=_Obhhh4o8t93v83EaYCRyA&bvm=bv.50310824,d.Yms`, reviewed 21.8.2013 , reviewed 06/08/2013

[9] `http://www4.nau.edu/microanalysis/Microprobe-SEM/Images/IonPump.jpg`,reviewed 1.8.2013

[10] Prof. Dr.-Ing. Volker Hinrichsen : Der elektrische Durschlag von Gasen, Technische Universität Darmstadt, Fachgebiet für Hochspannungstechnik

[11] `http://en.wikipedia.org/wiki/Paschen%27s_law`,reviewed 23.7.2013 , reviewed 28/7/2013

[12] `http://chemed.chem.wisc.edu/chempaths/GenChem-Textbook/Potential-Energy-898.html`, reviewed 11.8.2013

[13] `http://www2.uni-siegen.de/~pciii/PC23.pdf`, reviewed 25.8.2013

[14] S. Califano,Schwingungszustände, Wiley, 1976

[15] Prof. Dr. Gert Denninger : Das Quadrupol-Massenfilter, Universität Stuttgart, `http://www.pi2.uni-stuttgart.de/official/g.denninger/EXP_SS2004/PDF/qms.pdf`, reviewed 2.8.2013

[16] Timo Stängler : Restgasanalyse für den Elektronenkühlerteststand am Helmholtz-Institut Mainz

[17] http://ecee.colorado.edu/~bart/book/book/chapter2/ch2_3.htm,http://www.halbleiter.org/en/fundamentals/conductors/, reviewed 7.8.2013

[18] http://ecee.colorado.edu/~bart/book/book/chapter2/ch2_3.htm, reviewed 7.8.2013

[19] http://www.halbleiter.org/en/fundamentals/conductors/, reviewed 12.8.2013

[20] https://de.wikipedia.org/wiki/CCD-Sensor, reviewed on 16.8.2013

[21] http://www.microscopyu.com/articles/digitalimaging/images/ccdintro/ccdintrofigure2.jpg, reviewed 20.8.2013

[22] http://www.pixcellent.com/Image9.gif, reviewed 4.9.2013

[23] *SBIG Astronomical Instruments data sheet : ST-402ME, 2011*

[24] Jan-Eike von Seggern : ALPS II Technical Design Report, 2012, arXiv:1302.5647

[25] Private communication

[26] http://www.thorlabs.de/images/TabImages/Uncoated_N-BK7_Transmission.xlsx, reviewed 31.8.2013

[27] http://www.vpglass.com/filter_glass/images/rg850.gif, reviewed 31.8.2013

[28] http://www.uqgoptics.com/pdf/Schott%20RG850.pdf, reviewed 31.8.2013

[29] http://www.thorlabs.de/newgrouppage9.cfm?objectgroup_id=1000, reviewed 31.8.2013

[30] http://www.thorlabs.de/images/popupimages/FL051064-10.xlsx, reviewed 31.8.2013

[31] http://www.princetoninstruments.com/Uploads/Princeton/Documents/Datasheets/PIXIS/Princeton_Instruments_PIXIS_1024_eXcelon_rev_N3_8.21.2012.pdf, reviewed 11.8.2013

[32] http://www.heliosoptical.net/assets/images/BG40ltrans.gif, reviewed 31.8.2013

[33] Private communication with Corinna Peitzmann, MVS, DESY

[34] http://learn.hamamatsu.com/articles/images/frametransferccd.jpg, reviewed 3.9.2013